REPORT No. 690

LONGITUDINAL STABILITY AND CONTROL WITH SPECIAL REFERENCE TO SLIPSTREAM EFFECTS

By S. KATZOFF

SUMMARY

Data obtained in the N. A. C. A. full-scale wind tunnel concerning the effects of interference and of propeller operation on longitudinal stability and control have been studied. The data include pitching moments for various power conditions for airplanes with tails removed and with tails set at various stabilizer and elevator angles. A number of surveys of the dynamic pressure and the flow direction in the region of the horizontal tail surface are also included. Results are given for eight airplanes, including a model of a four-engine airplane tested both as a tractor and as a pusher and a model of a two-engine pusher. The effects are shown of propeller operation on the downwash angles and the dynamic pressures at the tail and on the pitching-moment contribution of the propeller and the wing.

INTRODUCTION

A large amount of data concerning the effects of propeller operation on longitudinal stability and control has been obtained in the N. A. C. A. full-scale wind tunnel. Included are power-off and power-on pitching moments for airplanes with the horizontal tail surfaces removed and with the tail surfaces set at various stabilizer and elevator angles. Some surveys of the dynamic pressures and the stream angles in the region of the horizontal tail surface are also included. Most of the data were, however, obtained incidental to tests made for other purposes and accordingly are of varying degrees of completeness.

As part of a general investigation directed toward a rational system of tail design, an analysis has been made of the data for each airplane with the purpose of evaluating the various interference and slipstream effects. Data were available on the following six single-engine airplanes: a Douglas YO–31A two-place observation airplane with parasol-wing arrangements; a McDonnell two-place low-wing monoplane; a Curtiss SOC–1, a Curtiss XSBC–3, and a Vought XO4U–2 two-place biplane; and a Vought SB2U–1 low-wing monoplane. In addition, data had been obtained from tests of a four-engine monoplane model of approximately 37-foot span arranged both as a tractor and a pusher airplane and from tests of a two-engine pusher monoplane model of 35-foot span.

The discussion has been mainly centered about the following points, which are of fundamental importance in tail-surface design:

(1) The characteristics of the isolated horizontal tail surface.

(2) The effect on these tail-surface characteristics of the position of the horizontal tail relative to the fuselage and the vertical tail.

(3) The influence of the wing and the fuselage wakes and of the propeller slipstream on the elevator effectiveness.

(4) The downwash angle, particularly as affected by propeller operation.

(5) The effect of flap deflection on the pitching moment for various conditions of propeller operation.

(6) The effect of propeller operation on the pitching moment of the airplane with tail removed.

A description of the wind tunnel and details of the methods of correcting the data are given in references 1, 2, and 3. The tunnel air speed for the tests was about 60 miles per hour except for a few cases in which it was varied in order to attain desired values of V/nD. Descriptions of the airplanes are included in the subsequent sections.

SYMBOLS

C_L lift coefficient.

C_D drag coefficient.

C_N normal-force coefficient.

C_m coefficient of pitching moment about the center of gravity.

$C_{m_{a.c.}}$ coefficient of pitching moment about the aerodynamic center.

$T_c' = \dfrac{\text{effective thrust}}{1/2\ \rho V^2 S_w}$ thrust coefficient based on wing area.

$T_c = \dfrac{\text{effective thrust}}{\rho V^2 D^2}$ thrust coefficient.

S_w wing area.

ρ air density.

V air speed.

n propeller revolution speed.

D propeller diameter.

q dynamic pressure, $1/2\ \rho V^2$.

q_0 free-stream dynamic pressure.

δ deflection of movable surface.

α angle of attack.

$(q/q_0)_{eff}$ effective dynamic-pressure factor, the ratio of measured $dC_m/d\delta_e$ to the value corresponding to free-stream dynamic pressure at the tail, as calculated from the characteristics of the tail surface alone, with allowance for cut-outs for the fuselage and the vertical tail.

$(q/q_0)_{av}$ ratio of average dynamic pressure at the tail, as found from air-flow surveys, to free-stream dynamic pressure. The average is weighted according to chord.

ϵ local downwash angle.

ϵ_{eff} effective downwash angle at the tail, as found by comparison of pitching moments with and without the horizontal tail.

ϵ_{av} average downwash angle at the tail, as found from air-flow measurements. The average is weighted according to both chord and dynamic pressure.

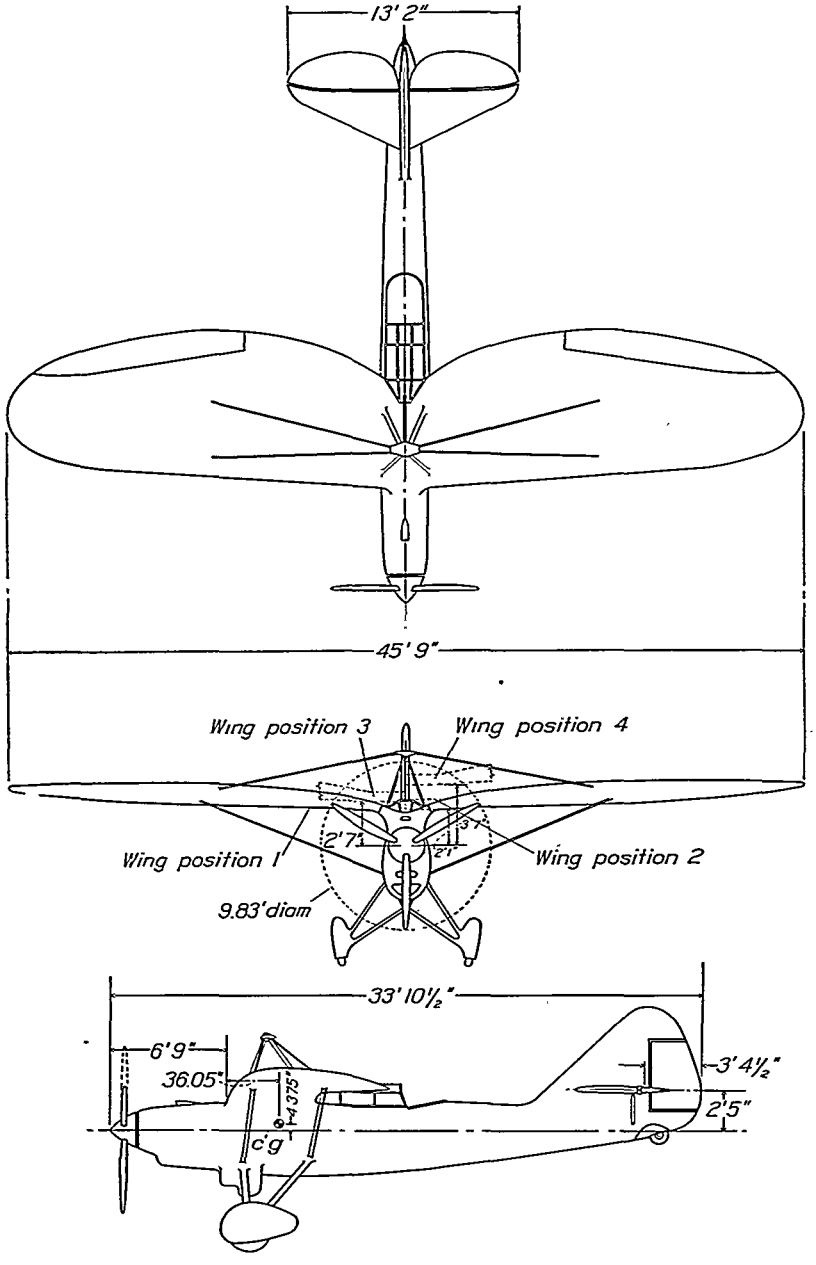

FIGURE 1.—Three-view drawing of the YO-31A airplane. The three parasol-wing positions are shown dotted. Areas, in square feet: wing, 337.5; horizontal tail, 48.7; gross elevator, 22.8; elevator back of hinge, 18.2.

Subscripts:

t horizontal tail.
e elevator.
s stabilizer.
f flap.
b balance.

THE YO-31A AIRPLANE

The YO-31A two-place observation airplane is shown in figure 1. Its normal arrangement provides for a gull wing but, in some of the tests, the wing was raised and a center section was added, the airplane being thereby transformed to the parasol type. Three different wing heights were used with this arrangement; their number designations are given in figure 1. Force tests were made of:

(1) The horizontal tail surface alone.

(2) The fuselage with the vertical tail surface attached.

(3) The fuselage and the complete tail assembly.

(4) The airplane complete with the exception of the horizontal tail surface.

(5) The complete airplane.

The tests for items (2) to (5) were made both with the propeller removed and with the propeller operating over a T_c' range from 0 to 0.32. For item (4), in addition to the force tests, surveys were made of the air flow in the vertical plane of the elevator hinge. The following analysis of the data treats the slipstream effects and the correlation of the characteristics of the horizontal tail surface installed on the airplane with those found for the isolated tail surface.

Horizontal tail surface.—The horizontal tail, mounted on the balance supports, is shown in figure 2. In figures 3, 4, and 5 are shown the lift, the drag, and the pitching-moment coefficients. Figure 5 also shows the positions of the aerodynamic center corresponding to the various elevator deflections; the aerodynamic center is at about the average quarter-chord position for elevator angles from 20° to −20°. Although the pitching moment of the tail surface itself has generally been neglected in stability and control studies, it appears to be appreciable. Thus, in the case of the YO-31A airplane, deflection of the elevator causes a change in pitching moment of about 6 percent more than that due to the change in the lift of the tail.

Fuselage and vertical tail surface.—The lift, the drag, and the pitching-moment coefficients of the combination of the fuselage and the vertical tail, for the propeller removed and for $V/nD=0.7$ and 0.5 ($T_c'=0.13$ and 0.32) are shown in figure 6. The coefficients are based on the wing area and the pitching-moment

FIGURE 2.—The YO-31A tail surface mounted in the N. A. C. A. full-scale wind tunnel.

coefficients are computed with respect to the center of gravity of the entire airplane (wing position 1, see fig. 1). The pitching moment for propeller removed is negative up to 12° angle of attack, probably because of the drag of the landing gear. For the two propeller-operating conditions, there is a pronounced increase

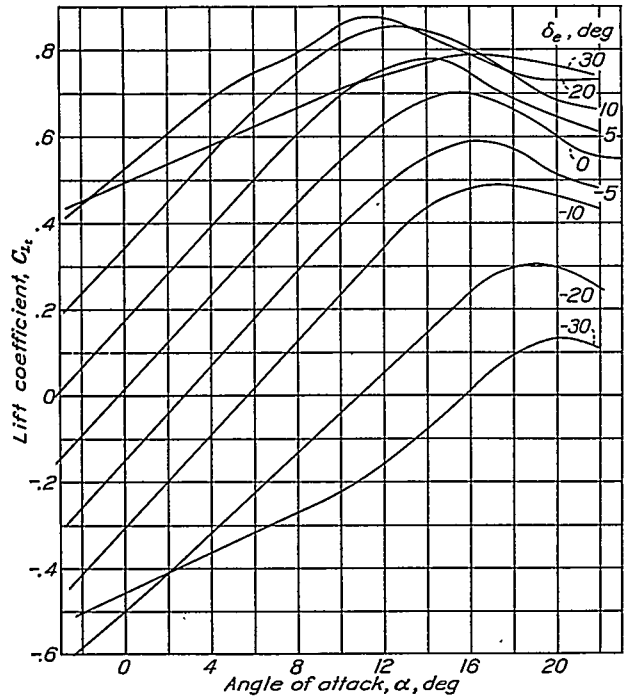

FIGURE 3.—Lift curves for the YO-31A tail surface at different elevator angles.

in the slope of the lift curve. Part of this increase is probably due to the effect of the slipstream on the fuselage. Most of it, however, corresponds merely to the vertical force on the inclined propeller. Thus, the vertical force indicated in reference 4 accounts for about 85 percent of the observed increase in lift; the vertical force indicated in reference 5 accounts for nearly 100 percent of it.

Fuselage and complete tail assembly.—A comparison of the results for the tail alone and the fuselage alone

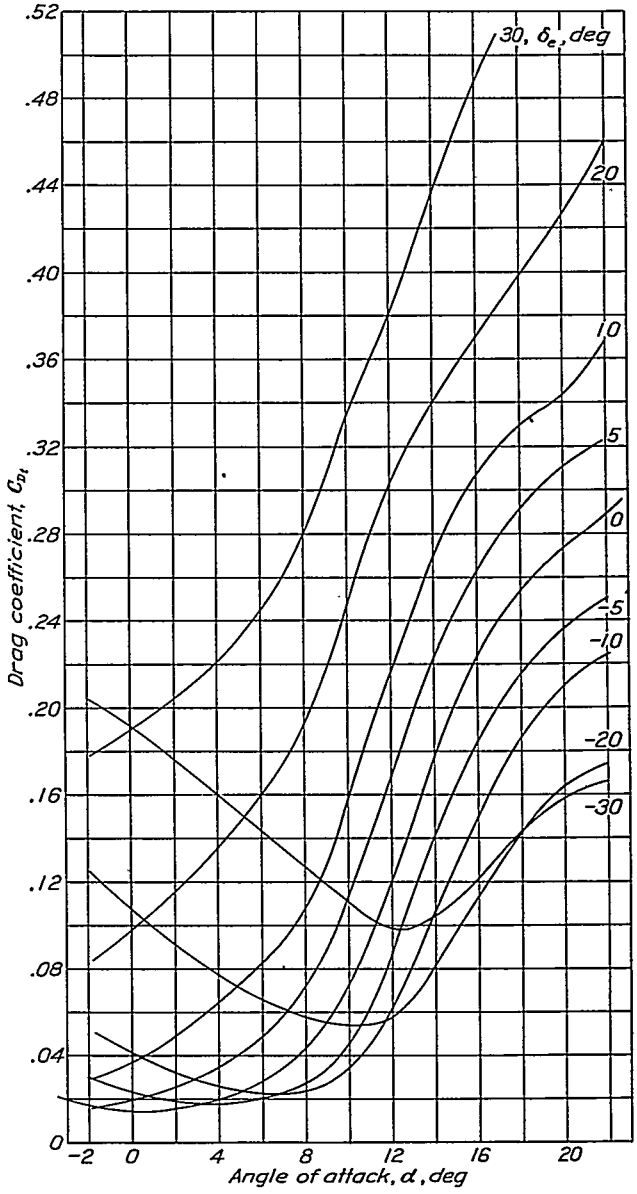

FIGURE 4.—Drag curves for the YO-31A tail surface at different elevator angles.

with those for the tail-fuselage combination made it possible to investigate the interference effects of the fuselage and the effects of the slipstream on the dynamic pressure and on the air-flow direction at the tail.

Figure 7 shows some typical curves of lift, drag, and pitching-moment coefficients against elevator angle for propeller removed and propeller operating ($T_c'=0.32$). The pitching-moment increments due to the tail are shown for four angles of attack in figure 8. For comparison, are also shown the increments calculated by applying the measured lift and drag increments at the

aerodynamic center with an allowance for the pitching moment of the tail surface about its aerodynamic center. The agreement is satisfactory, indicating that the position of the aerodynamic center is unchanged by the presence of the fuselage.

From the same set of data are determined the effective dynamic-pressure factor $(q/q_0)_{eff}$ and the effective downwash angle ϵ_{eff}. Thus, for $\alpha=-0.6°$ and propeller removed, calculations showed that, if free-stream dynamic pressure existed at the tail and the tail characteristics were unaltered by the presence of the fuselage, the value of $dC_m/d\delta_e$ should be -0.0130 at $\delta_e=0°$. The experimental value is -0.0116, or only 89 percent of the calculated value. The reduction in area caused by the passage of the horizontal tail through the vertical tail, however, accounts for a loss of 6 percent. The rest of the loss, 5 percent, is ascribed to the reduction in

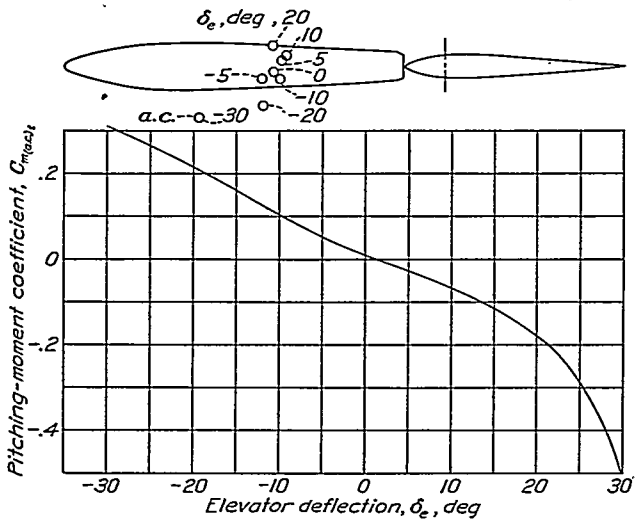

FIGURE 5.—Variation of pitching-moment coefficient with elevator angle, and position of aerodynamic center for different elevator angles. The YO-31A tail surface.

dynamic pressure at the tail. The value of $(q/q_0)_{eff}$ is thus 0.95. The effective downwash angle ϵ_{eff} is found by applying the tail-surface data and the factor $(q/q_0)_{eff}$ to the difference between the pitching moments for the tail-on and the tail-off conditions.

Curves for $(q/q_0)_{eff}$ and ϵ_{eff} are given in figure 9 for propeller removed and propeller operating. Propeller operation raises the value of $(q/q_0)_{eff}$ and causes ϵ_{eff} to increase with angle of attack. The downflow for the propeller-removed condition is due partly to the tendency of the flow near the middle of the tail to follow the downward slope of the upper surface of the fuselage and partly to the downwash that must be associated with the lift of the fuselage.

It may be pointed out that these results pertaining to the downflow at the tail for the wing-removed condition have, in general, little direct applicability because the wing downwash, in the case of the complete airplane, will cause the average angle of attack of the fuselage with respect to the local air flow to be much less than its angle of attack with respect to the flight direction.

Airplane complete with the exception of the horizontal tail surface.—The foregoing analysis was repeated for the wing-on condition in order to determine the effects of the wing on the downwash and the dynamic pressure at the tail. For simplicity in the interpretation of the results, the same center-of-gravity position was used in computing pitching moments for all four wing positions.

In figure 10 are shown the pitching-moment curves of the airplane with the propeller removed and with the propeller operating. The effect of propeller operation on the pitching moment is seen to be nearly the same for all four wing positions. Furthermore, the effect is nearly the same as in the case of the wing removed (cf. fig. 6); that is, the effect of propeller operation on

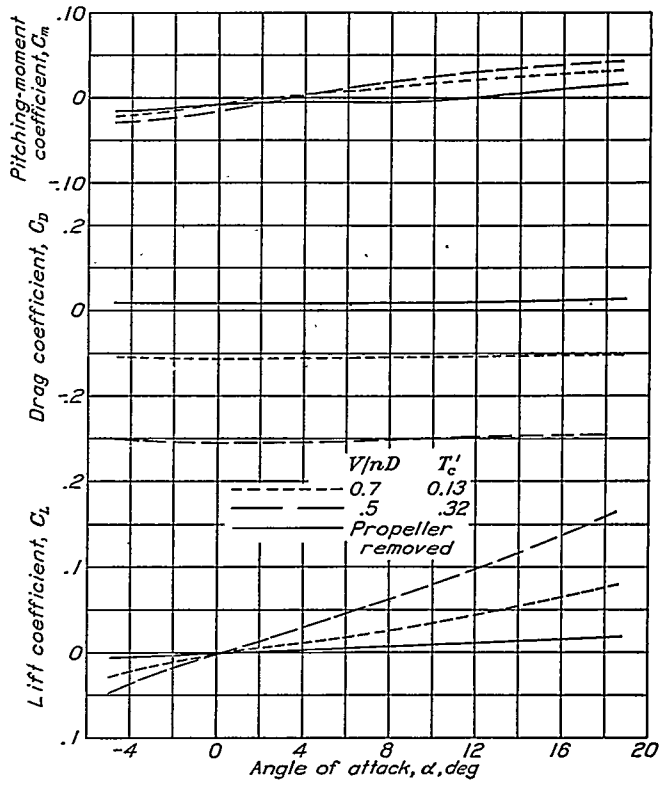

FIGURE 6.—Effect of propeller operation on the lift, the drag, and the pitching-moment coefficients. The YO-31A fuselage and vertical tail (wing and horizontal tail removed); $T_c=1.75\ T_c'$.

the pitching moment probably exists mainly at the propeller rather than at the wing.

Entire airplane.—Pitching moments were obtained for the entire airplane at different angles of attack, elevator angles, and propeller-operating conditions. Comparison of these pitching moments with the corresponding data for the airplane with the tail removed made possible the determination of $(q/q_0)_{eff}$ and ϵ_{eff} and their variation with angle of attack. The results are given in figures 11 and 12. Operation of the propeller increases both the effective dynamic pressure and the downwash angle at the tail.

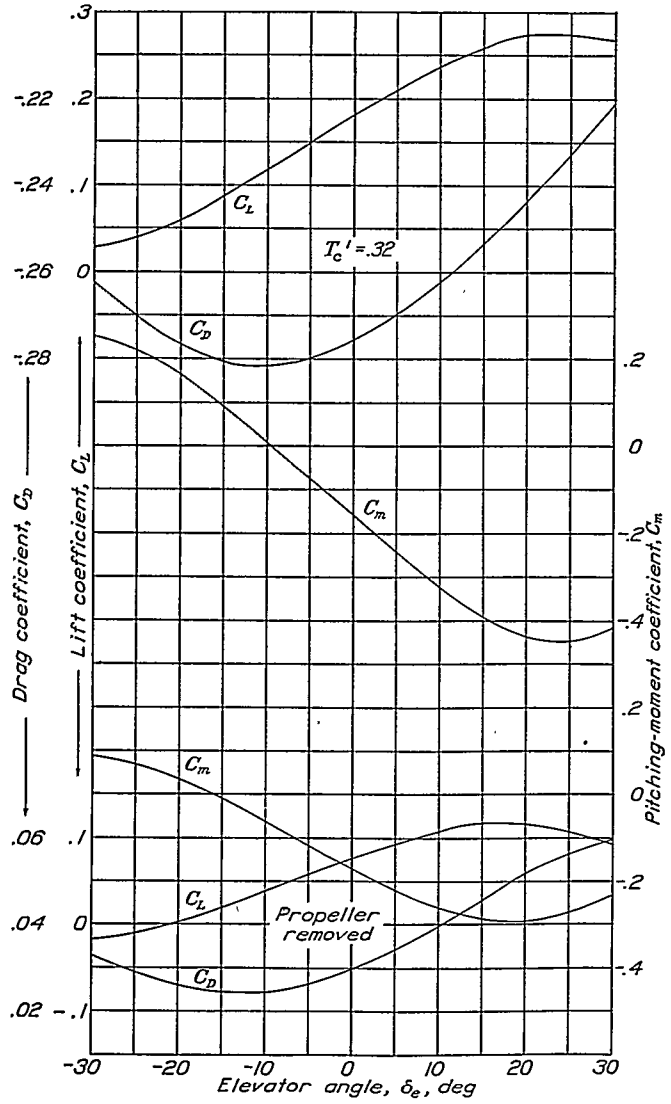

FIGURE 7.—Variation of lift, drag, and pitching-moment coefficients with elevator angle. The YO-31A fuselage and complete tail (wing removed); propeller removed and propeller operating; α, 12.2°; $T_c = 1.75\ T_c'$.

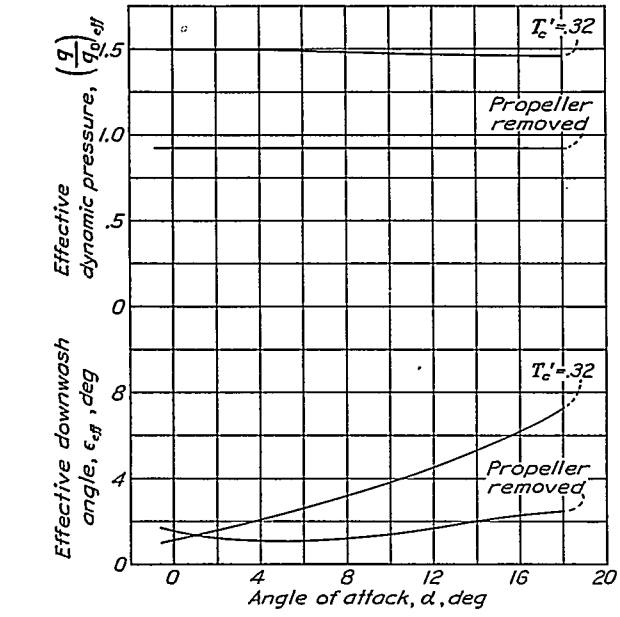

FIGURE 9.—Effect of propeller operation on the effective dynamic pressure and downwash angle at the tail. The YO-31A fuselage and complete tail (wing removed); $T_c = 1.75\ T_c'$.

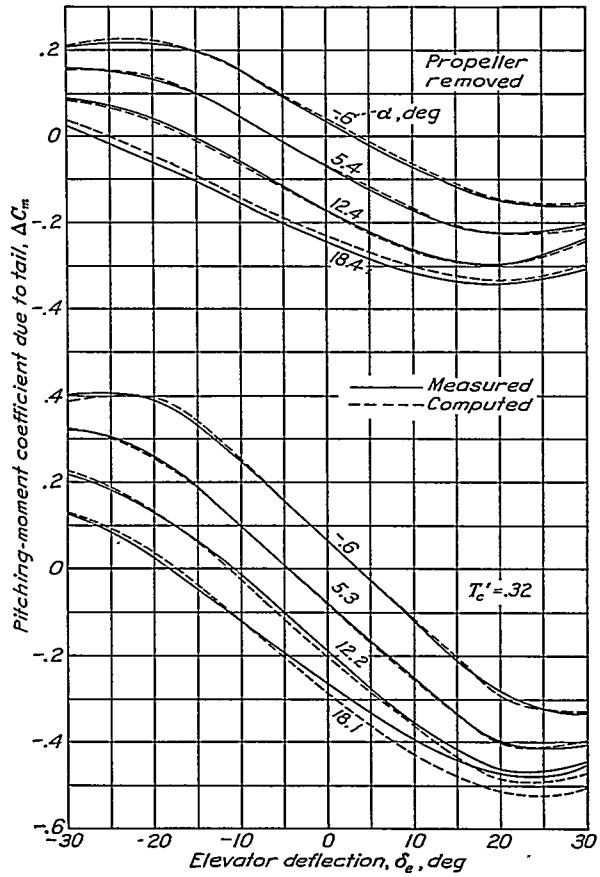

FIGURE 8.—Comparison of the measured pitching-moment coefficients and the pitching-moment coefficients computed from the tail forces. The YO-31A fuselage and complete tail (wing removed); propeller removed and propeller operating; $T_c = 1.75\ T_c'$.

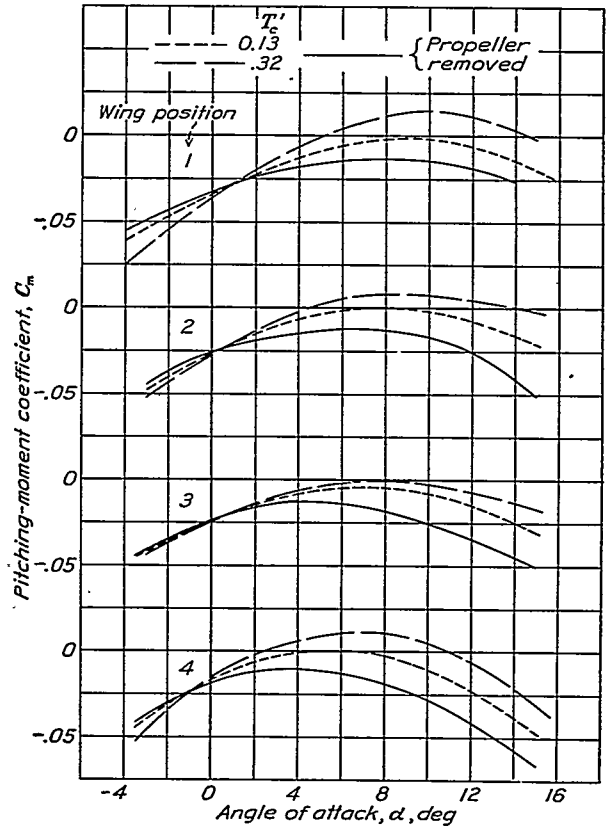

FIGURE 10.—Effect of propeller operation on the pitching-moment coefficient. The YO-31A airplane with horizontal tail removed; $T_c = 1.75\ T_c'$.

In one of the tests, pitching-moment measurements were made with three different stabilizer settings. Within experimental error, the results showed that the ratio of stabilizer effectiveness to elevator effectiveness, $\frac{dC_{L_t}}{d\delta_s}\Big/\frac{dC_{L_t}}{d\delta_e}$, was the same as for the tail alone.

Air-flow surveys.—In order to investigate the local velocities and the air-flow directions in the plane of the elevator hinge line, flow surveys were made in the plane of the elevator hinge line with the horizontal tail removed. The full-scale-tunnel survey head (reference 1) was used for these surveys, which consisted of measurements of the dynamic pressures and of the angles of pitch and yaw.

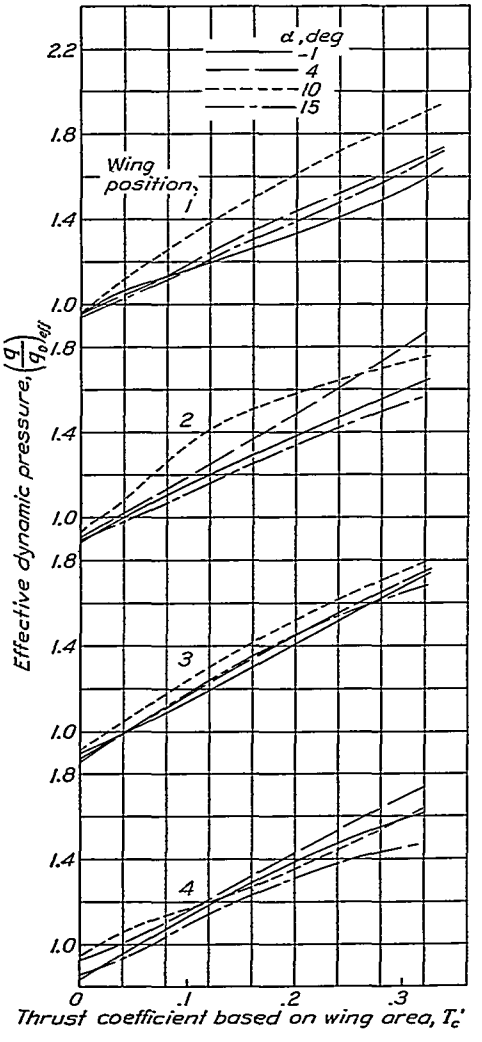

FIGURE 11.—Effect of propeller operation on the effective dynamic pressure at the tail. The YO-31A airplane; T_c=1.75 T_c'.

Representative results of the surveys for wing positions 1 and 4 are shown in the maps of figure 13. Measurements were made only at the points where the vectors are shown; values of dynamic pressure at other points were found by interpolation. Jet-boundary corrections for downwash were applied according to the method of reference 3. Comparison of figures 13 (a) and 13 (c) shows how the wing wake rises, relative to the tail, with angle of attack for the propeller-removed condition. The fuselage wake is clearly defined for wing position 4 (fig. 13 (e)) but not for wing position 1 (figs. 13 (a) and 13 (c)). The rotation of the slipstream is easily seen in figures 13 (d) and 13 (f), although its passage over the wing clearly causes considerable distortion.

The dynamic pressures and the downwash angles across the elevator hinge line for all the conditions for which surveys were made are plotted in figures 14 to 17.

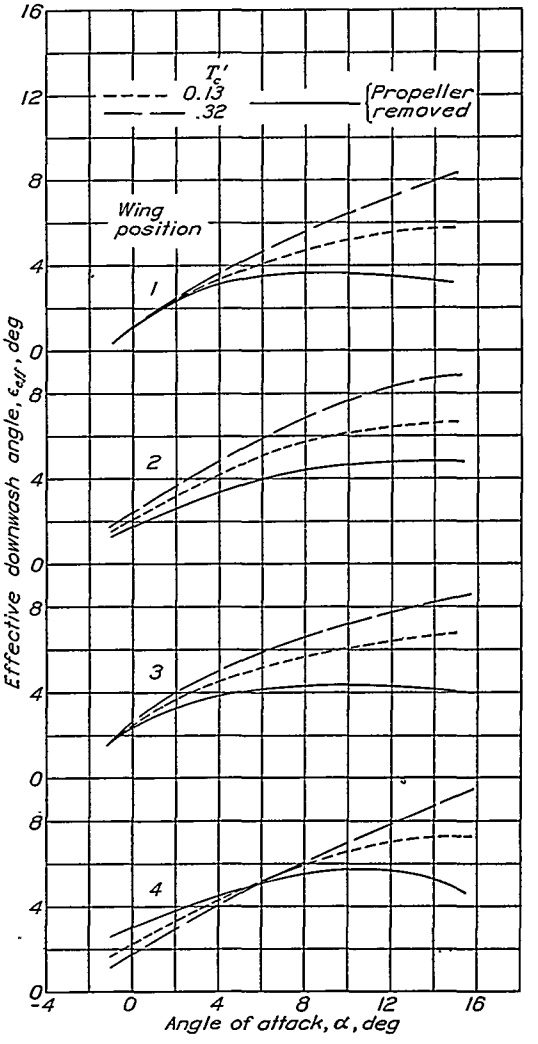

FIGURE 12.—Effect of propeller operation on the effective downwash angle at the tail. The YO-31A airplane; T_c=1.75 T_c'.

No readings were available at distances less than 1.5 feet from the airplane center line; the center sections of the curves are therefore left open. In the computation of the values of $(q/q_0)_{av}$ and ϵ_{av}, however, the center sections were interpolated. These values are given in the following table, together with the corresponding values of $(q/q_0)_{eff}$ and ϵ_{eff}.

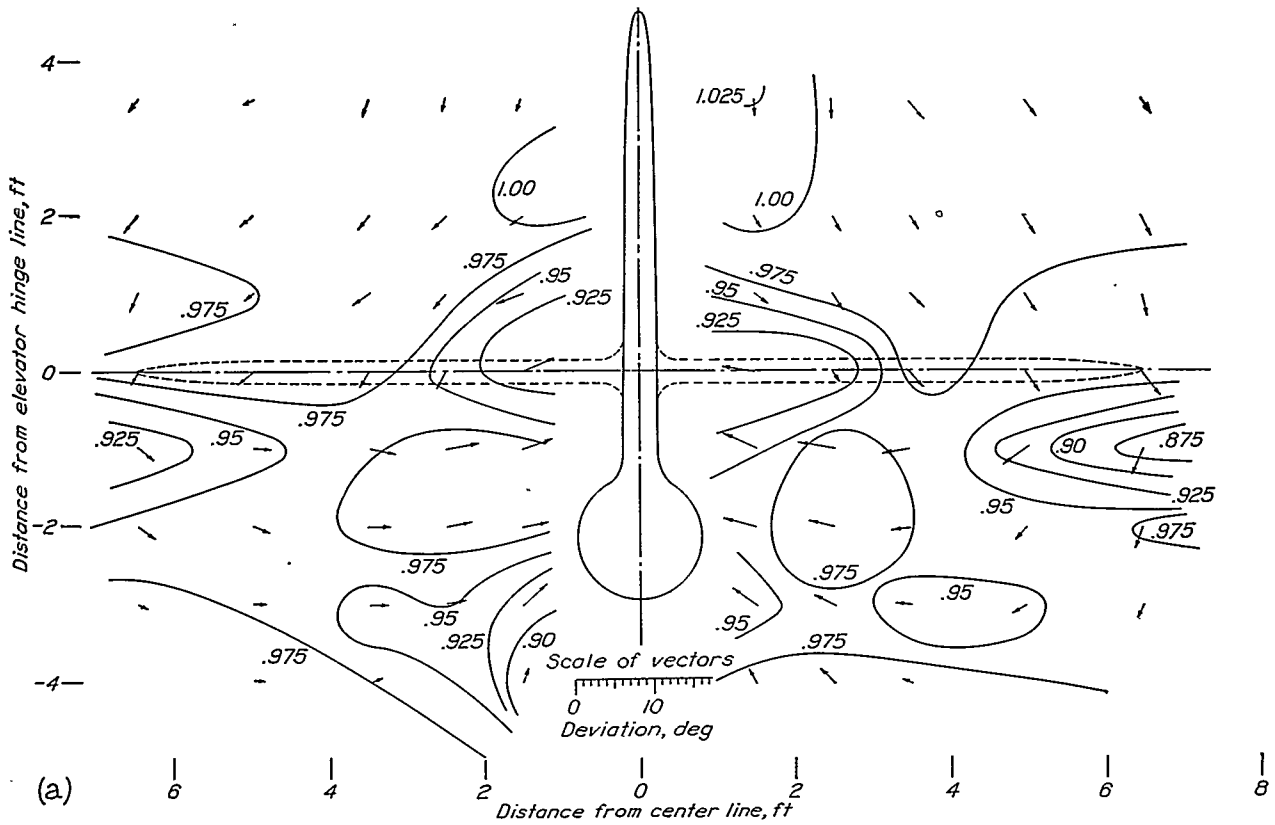

(a) Wing position 1; propeller removed; α, −0.9°.

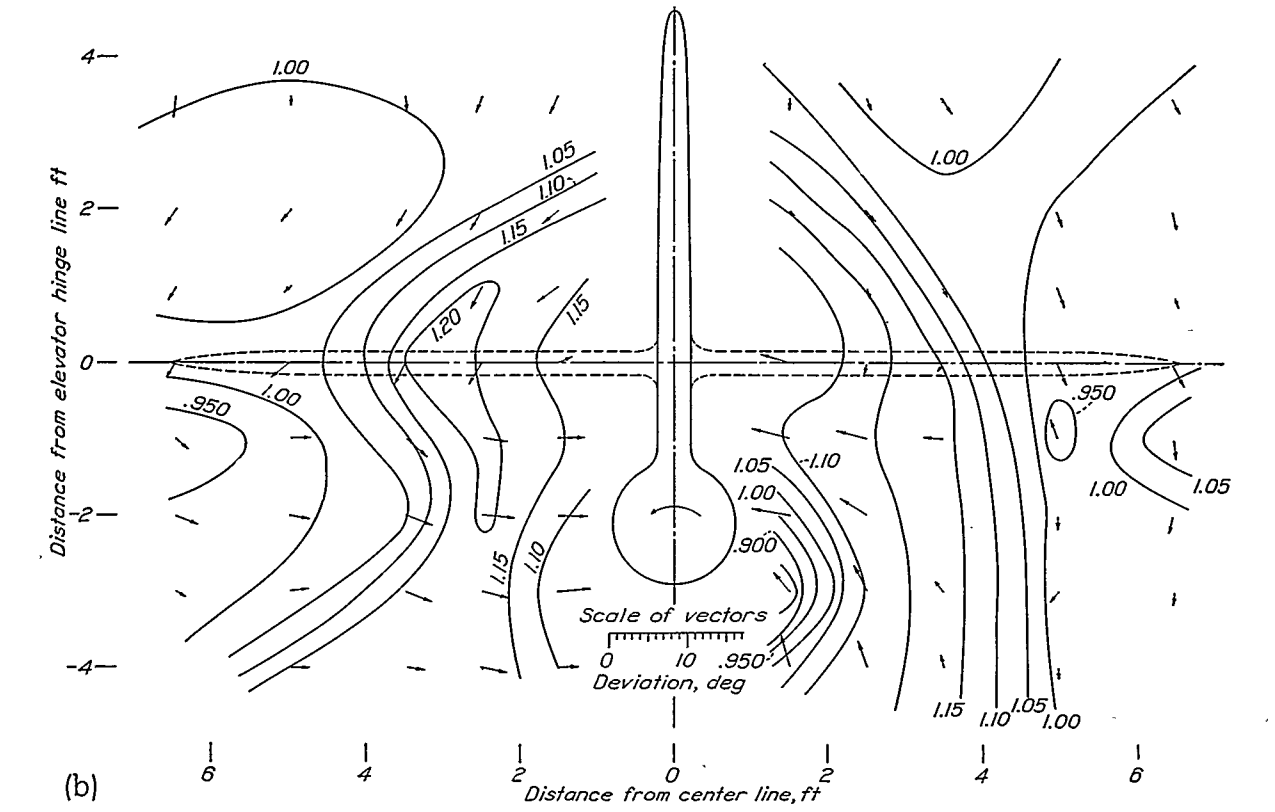

(b) Wing position 1; V/nD, 0.96; T_c', 0.034; T_s, 0.059; α, −1.0°.

FIGURE 13.

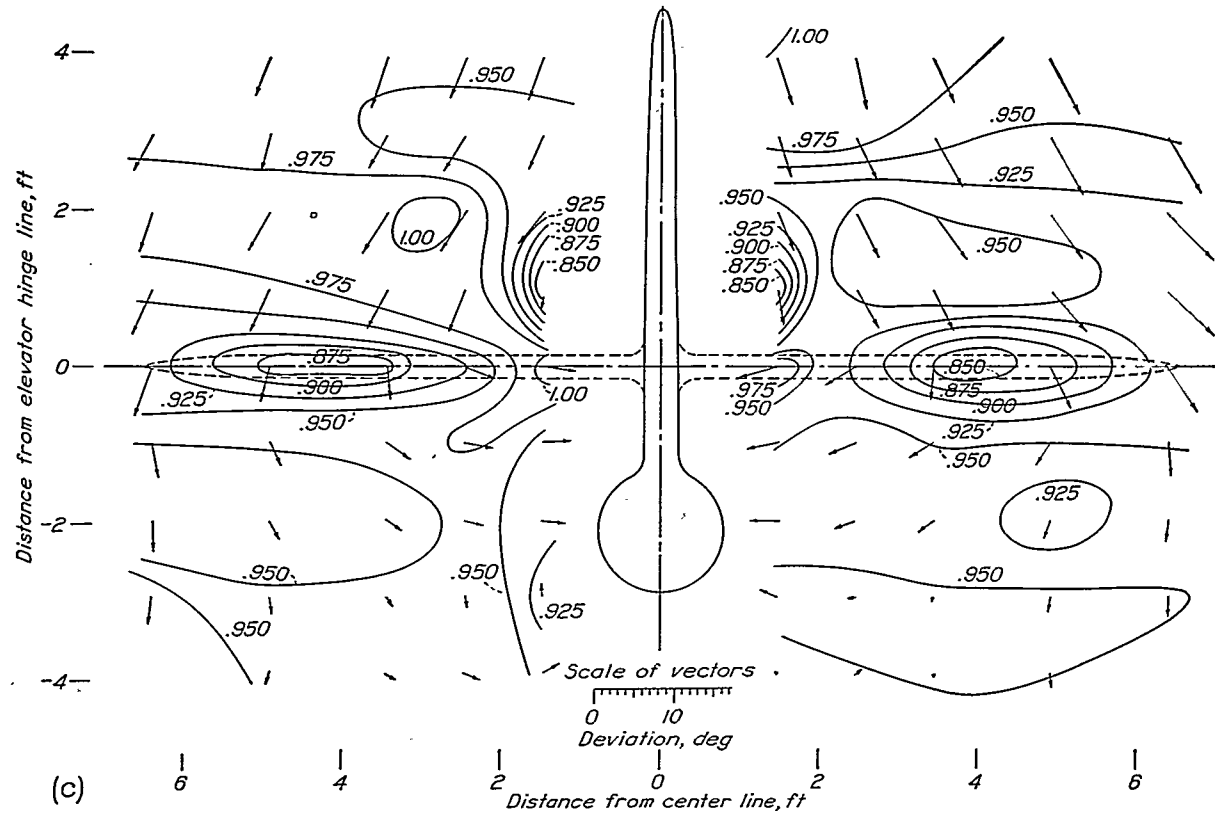

(c) Wing position 1; propeller removed; α, 3.9°.

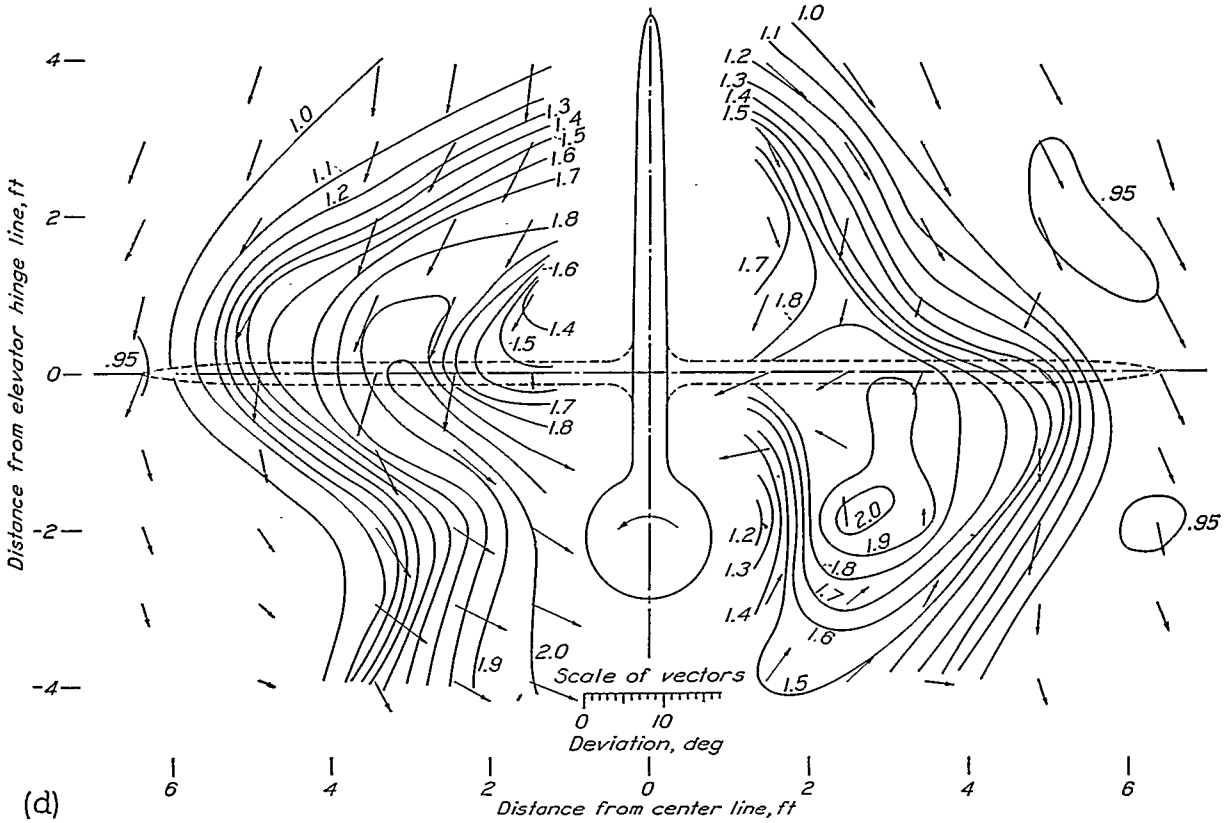

(d) Wing position 1; V/nD, 0.67; T_c', 0.139; T_c, 0.243; α, 3.8°.

FIGURE 13.

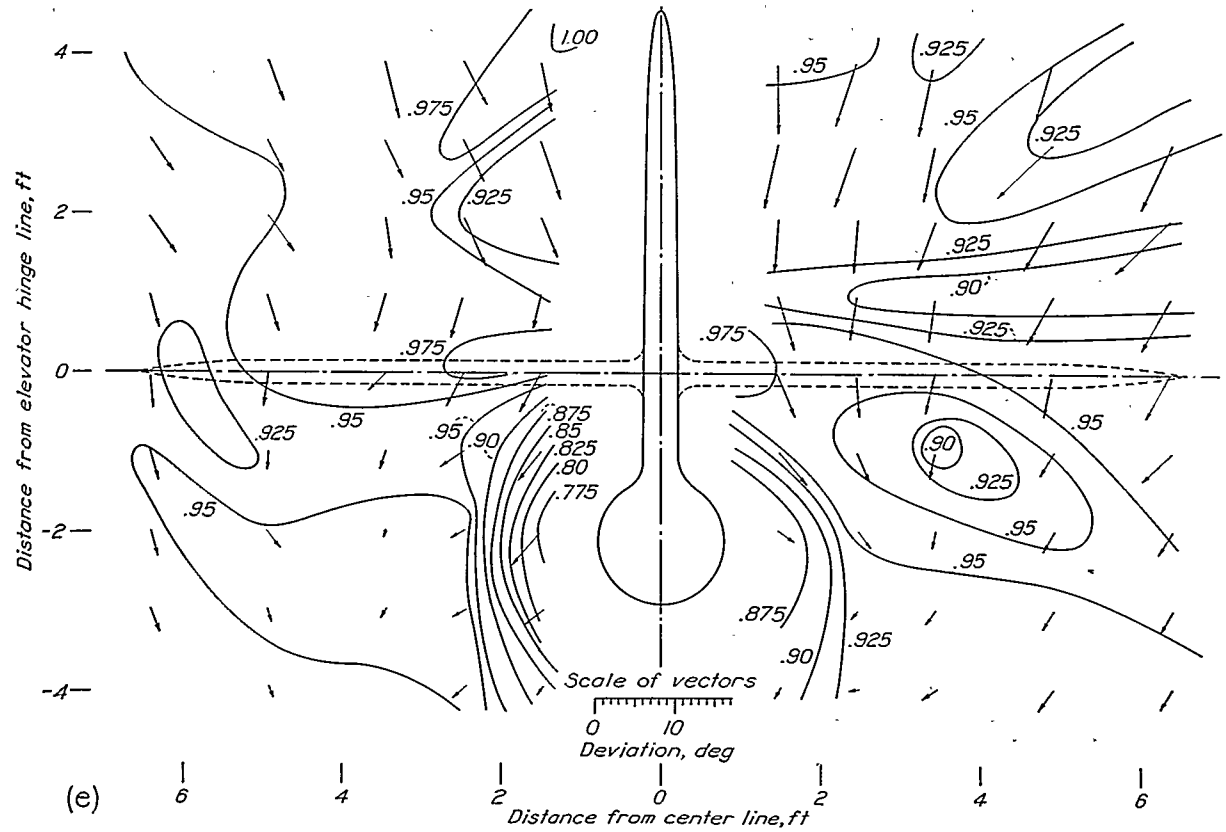

(e) Wing position 4; propeller removed; α, 4.2°.

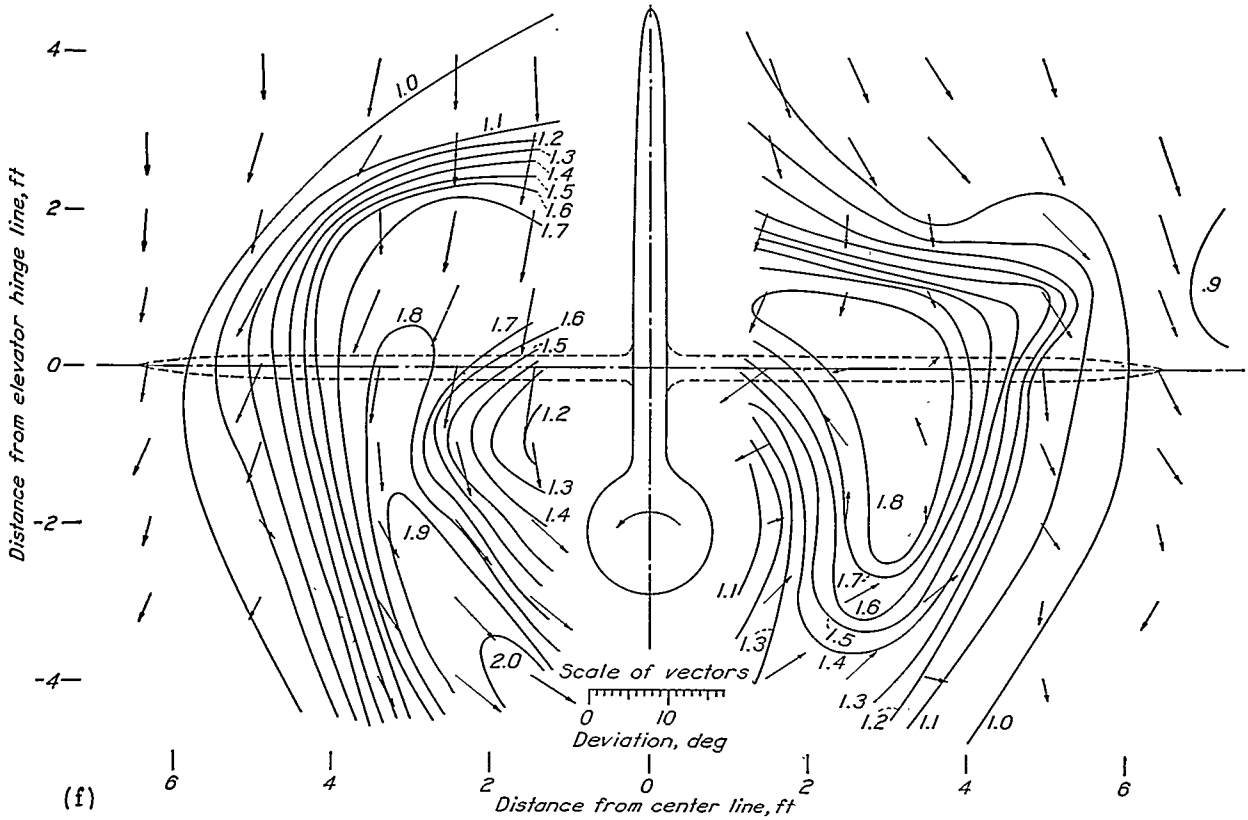

(f) Wing position 4; V/nD, 0.67; T_c', 0.134; T_c, 0.234; α, 4.1°.

FIGURE 13.—Dynamic-pressure (q/q_0) contours and inclination of the air stream in the plane of the elevator hinge line. Vectors show deviation of air flow from the free-stream direction. View looking forward. The YO-31A airplane with horizontal tail removed.

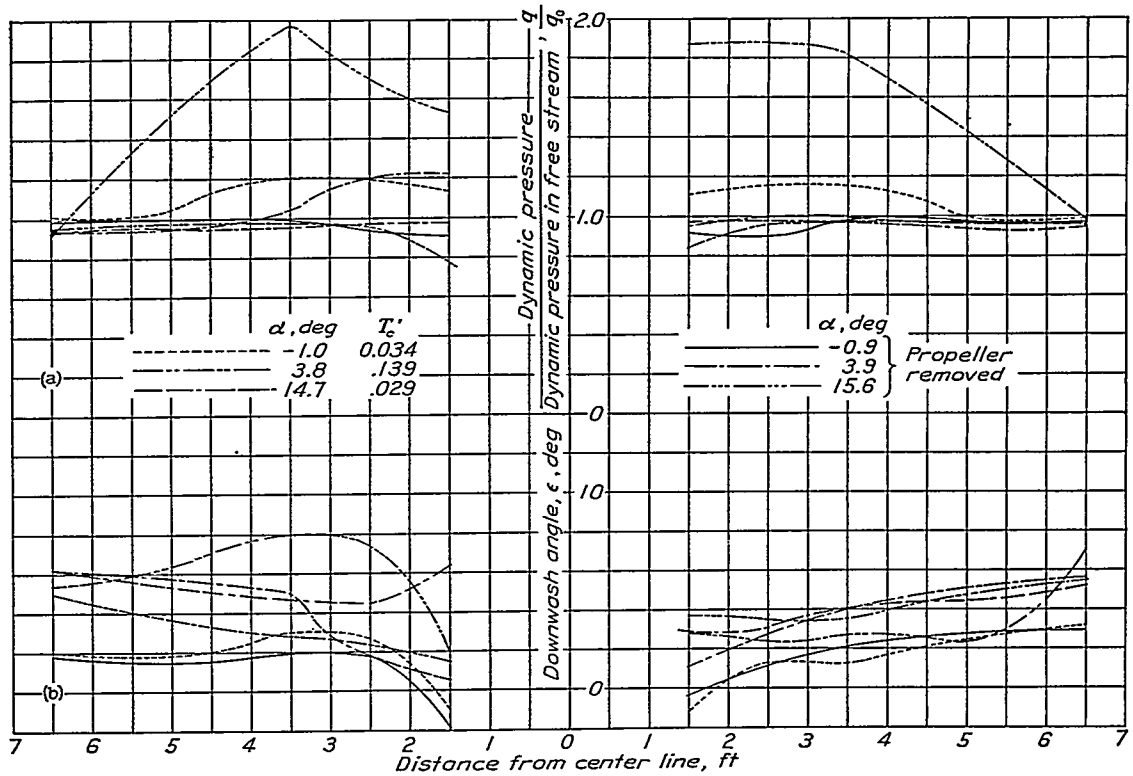

(a) Dynamic pressures across the elevator hinge line.
(b) Downwash angles across the elevator hinge line.

FIGURE 14.—Dynamic pressures and downwash angles for the YO-31A airplane. Wing position 1; $T_c = 1.75\ T_c'$.

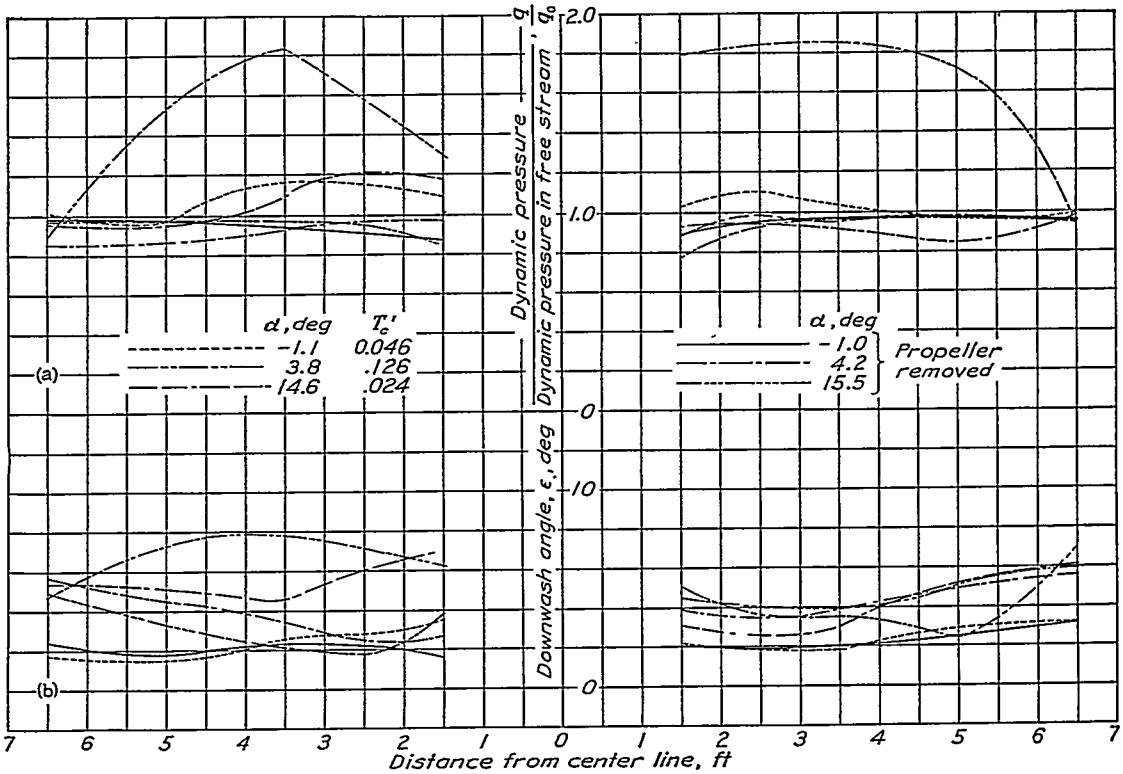

(a) Dynamic pressures across the elevator hinge line.
(b) Downwash angles across the elevator hinge line.

FIGURE 15.—Dynamic pressures and downwash angles for the YO-31A airplane. Wing position 2; $T_c = 1.75\ T_c'$.

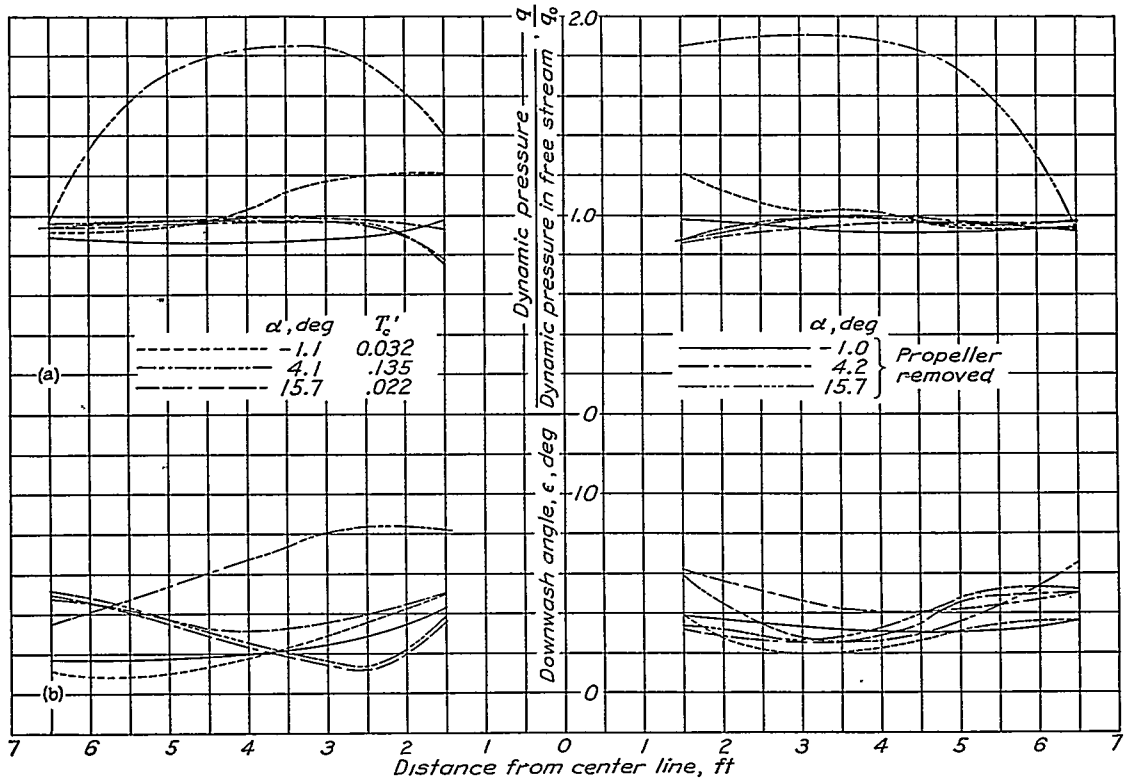

(a) Dynamic pressures across the elevator hinge line.
(b) Downwash angles across the elevator hinge line.

FIGURE 16.—Dynamic pressures and downwash angles for the YO-31A airplane. Wing position 3; $T_c=1.75\ T_c'$.

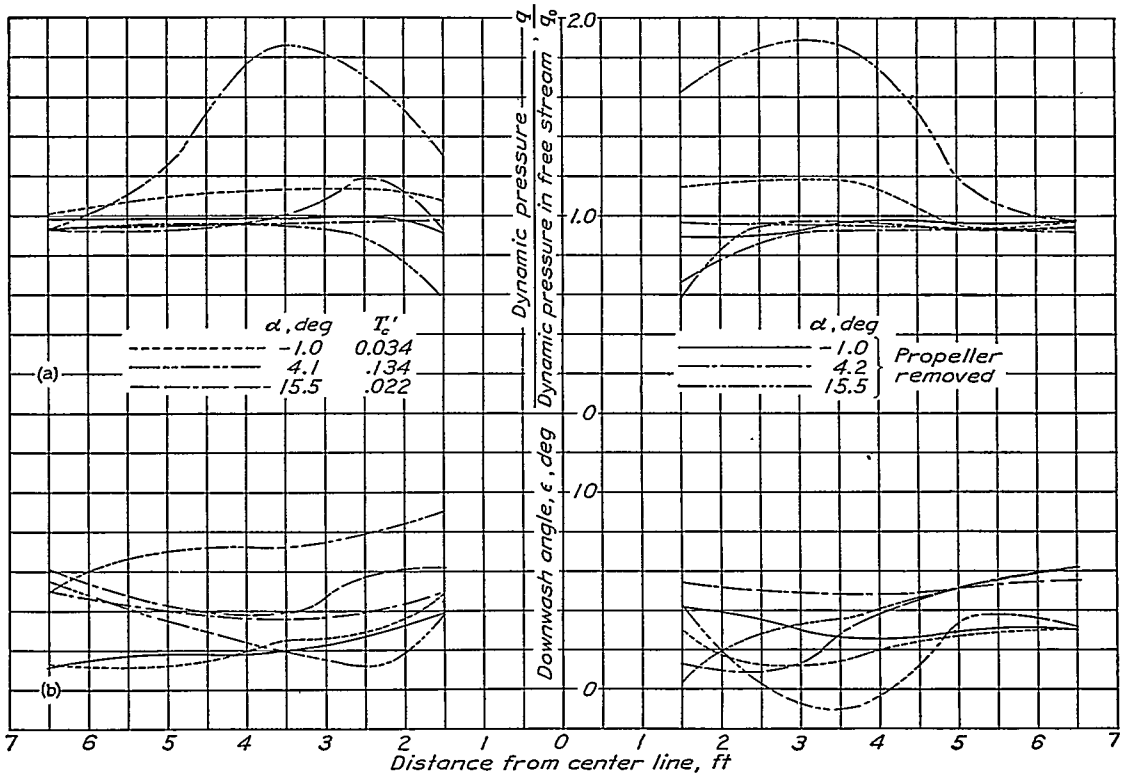

(a) Dynamic pressures across the elevator hinge line.
(b) Downwash angles across the elevator hinge line.

FIGURE 17.—Dynamic pressures and downwash angles for the YO-31A airplane. Wing position 4; $T_c=1.75\ T_c'$.

COMPARISON OF EFFECTIVE AND AVERAGE VALUES OF DYNAMIC PRESSURE AND DOWNWASH ANGLE AT THE TAIL FOR THE YO-31A AIRPLANE

Wing position	α (deg)	T_c' (a)	$(q/q_0)_{eff}$	$(q/q_0)_{av}$	ϵ_{eff} (deg)	ϵ_{av} (deg)
1	−0.9		0.94	0.93	2.6	0.9
	−1.0	0.034	1.05	1.08	2.4	1.1
	3.9		.95	.96	4.4	3.0
	3.8	.139	1.30	1.70	4.2	4.2
	15.6		.91	.91	4.6	3.3
	14.7	.029	1.01	1.03	5.5	4.6
2	−1.0		.87	.92	1.6	2.0
	−1.1	.046	.96	1.04	1.6	2.4
	4.2		.93	.91	3.6	3.6
	3.8	.126	1.27	1.79	4.4	4.8
	15.5		.90	.90	4.0	3.7
	14.6	.024	.94	1.02	4.7	4.5
3	−1.0		.91	.92	1.2	3.2
	−1.1	.032	.97	1.05	1.2	3.4
	4.2		.85	.92	3.2	4.6
	4.1	.135	1.27	1.71	4.2	5.7
	15.7		.86	.90	4.8	3.3
	15.7	.022	.93	.91	5.3	3.1
4	−1.0		.84	.93	.4	3.0
	−1.0	.034	.94	1.10	.4	2.8
	4.2		.92	.95	3.2	4.8
	4.1	.134	1.24	1.54	3.3	5.0
	15.5		.85	.80	3.2	3.0
	15.5	.022	.90	.90	4.0	4.0

[a] Missing values indicate that the propeller was removed.

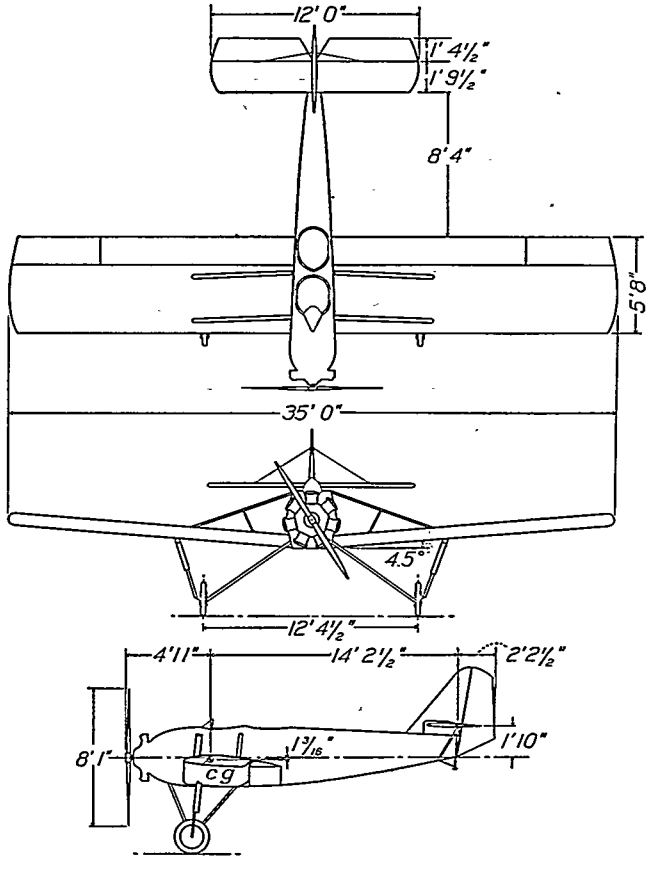

FIGURE 18.—Three-view drawing of the McDonnell airplane, original condition. Areas, in square feet: wing, 196.6; horizontal tail, 35.8; elevator, 14.8.

For the propeller removed or at the low thrust coefficients, the agreement between the average and the effective dynamic pressures is satisfactory. At the higher thrust coefficients, however, the effective value is considerably less than the corresponding average measured value. Thus, for wing position 1, where the slipstream increases the average dynamic pressure at the tail to 1.70 q_0, the effective dynamic pressure is increased to only 1.30 q_0. Although the discrepancy is large, reasons for it are not very clear. One of the causes is probably the jet-boundary effect of the slipstream, which is similar to that of an open wind tunnel. It is also very likely that the nonuniformity and the pulsation of the flow contribute to the low values of $(q/q_0)_{eff}$.

In the comparison between ϵ_{eff} and ϵ_{av}, the agreement appears to be satisfactory (within 1°) in about half the cases. The disagreement probably has the same causes

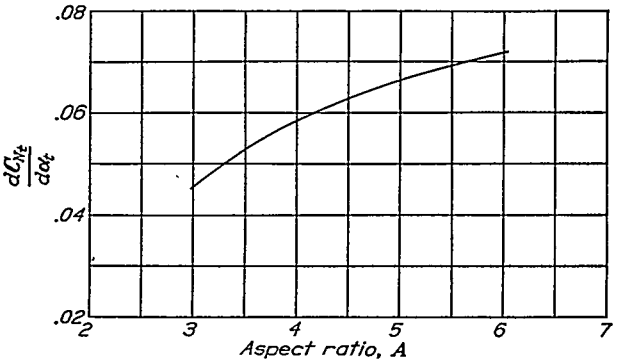

FIGURE 19.—Variation of lift-curve slope with aspect ratio, applicable to tail surfaces with normal-size cut-outs.

as the disagreement found in the comparison between $(q/q_0)_{eff}$ and $(q/q_0)_{av}$.

THE McDONNELL AIRPLANE

A three-view drawing of the McDonnell airplane is shown in figure 18. In the condition shown, pronounced and dangerous tail buffeting occurred. In some of the tests described in reference 6, however, the airplane was modified by placing fillets at the wing roots and by putting a cowling over the engine, which resulted in a marked improvement in performance.

For this airplane, as for those to be subsequently discussed, no tests were made of the isolated tail surface. Reasonable estimates of the characteristics of the isolated tail surface were obtained from figures 21 and 26 of reference 7, which are herein reproduced as

figures 19 and 20. The lack of experimental data for the actual tails used, however, may materially lower the accuracy of the analyses, in comparison with the analysis for the YO–31A airplane. The procedure has been somewhat simplified by considering the tail forces to consist only of the normal force, applied at the aerodynamic center, and the pitching moment about the aerodynamic center, so that the chordwise force is neglected.

The characteristics of the isolated tail surface are estimated to be

$$dC_{N_t}/d\delta_s = 0.0593$$
$$dC_{N_t}/d\delta_e = 0.55 \times dC_{N_t}/d\delta_s = 0.033$$

The aerodynamic center is assumed to be at the quarter-chord point and the pitching-moment coefficient with respect to the aerodynamic center is assumed to be equal to that found for the YO–31A tail, $C_{m_{(a.c.)_t}} = -0.01\ \delta_e$. From these values and the geometry of the airplane, it follows that, if the properties of the tail surface were not subject to interference, $dC_m/d\delta_e$ would be −0.0147. The highest value experimentally found, for the case of the cowling over the engine and the airplane at a low angle of attack, was −0.0134, which is 9 percent lower than the computed value. About 2 percent may be accounted for by the area removed at the vertical tail, so that the effective dynamic pressure over the tail surface $(q/q_0)_{eff}$ is 0.93.

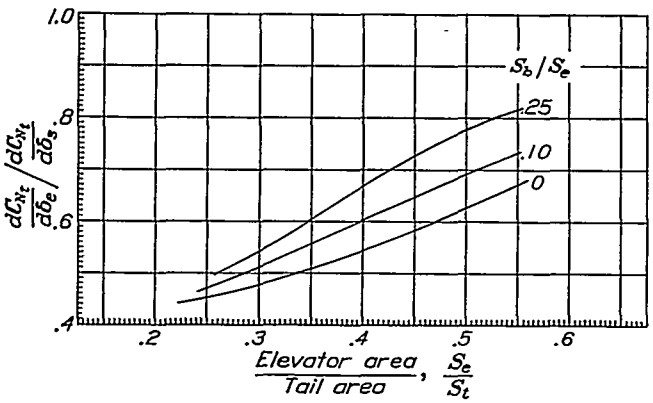

FIGURE 20.—Relative elevator effectiveness.

In figure 21, the maximum values of $dC_m/d\delta_e$ are plotted against angle of attack for the airplane in the original condition, with a cowling over the engine, with a large fillet at the wing-fuselage juncture, and with both the cowling and the fillet. For the power-off condition, the modifications that improved the air flow considerably increased the elevator effectiveness. Reduction in tail buffeting also paralleled the increase in $dC_m/d\delta_e$ (reference 6).

Values are also shown in figure 21 for the propeller-operating condition. The thrust was approximately

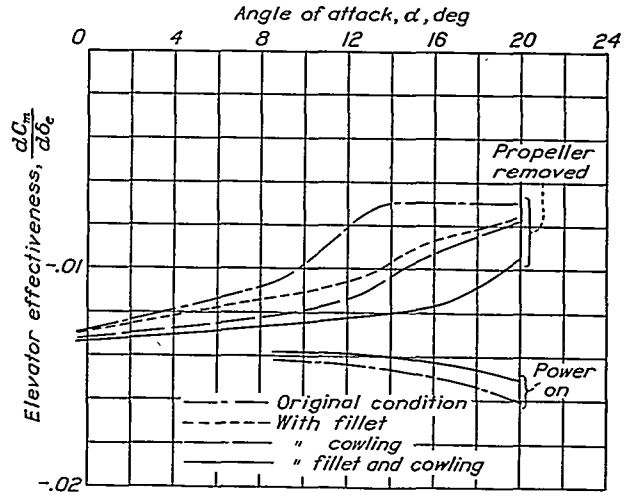

FIGURE 21.—Elevator effectiveness for different airplane and power conditions. The McDonnell airplane. Thrust for power-on conditions just sufficient for level flight.

equal to the drag and accordingly increased with angle of attack. Correspondingly, $dC_m/d\delta_e$ also increased slightly with angle of attack.

The results of air-flow surveys made in the plane of the elevator hinge line for a high angle of attack, both with the propeller removed and with the propeller operating, are shown in figure 22 for the airplane in its original condition and in its improved condition. Comparison of figure 22 (a) with figure 22 (c) shows that, for the propeller-removed condition, the addition of the fillet and the cowling results in a notable improvement in regularity of the air flow and a large increase in dynamic pressure. Operation of the propeller, however, tends to minimize this improvement. (Cf. figs. 22 (b) and 22 (d).)

In figure 23 are plotted the measured dynamic pressures and downwash angles across the elevator hinge line. The average values are given in the following table, together with the corresponding values of $(q/q_0)_{eff}$ and ϵ_{eff}, as found from pitching-moment measurements.

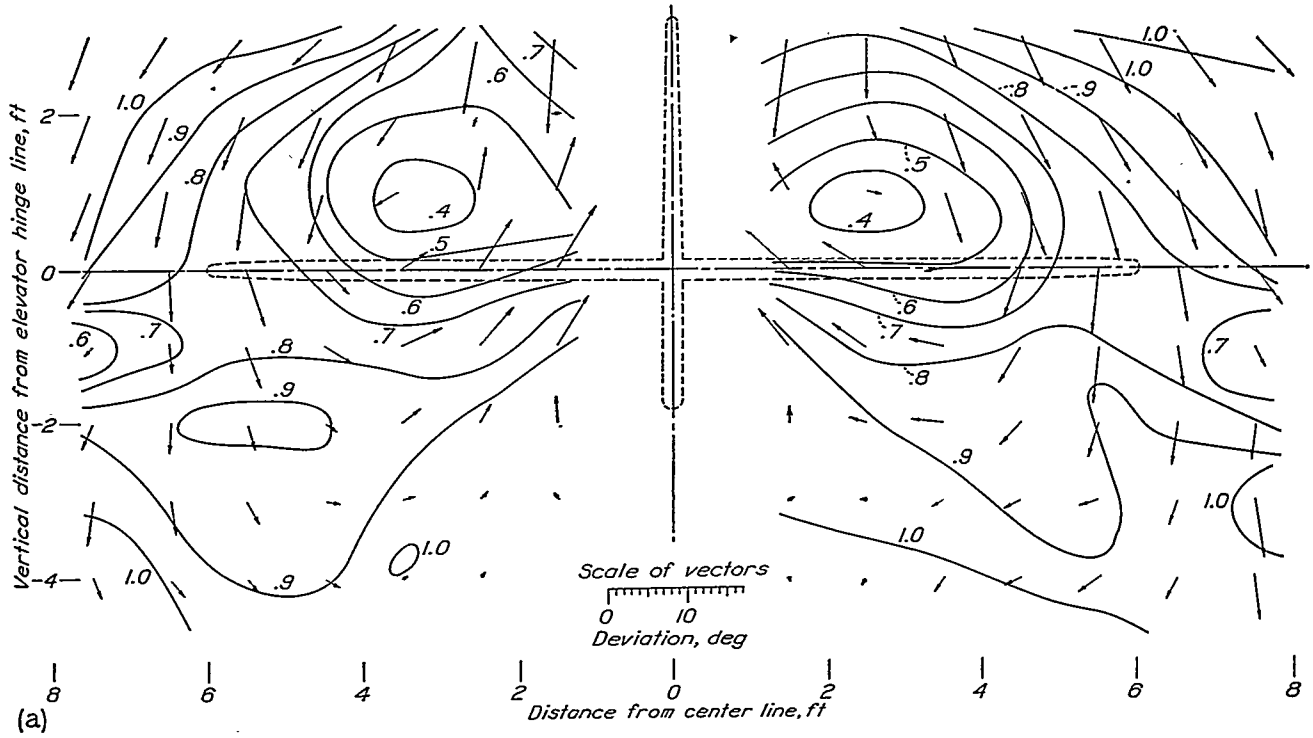

(a) Original condition; propeller removed; α, 14.2°.

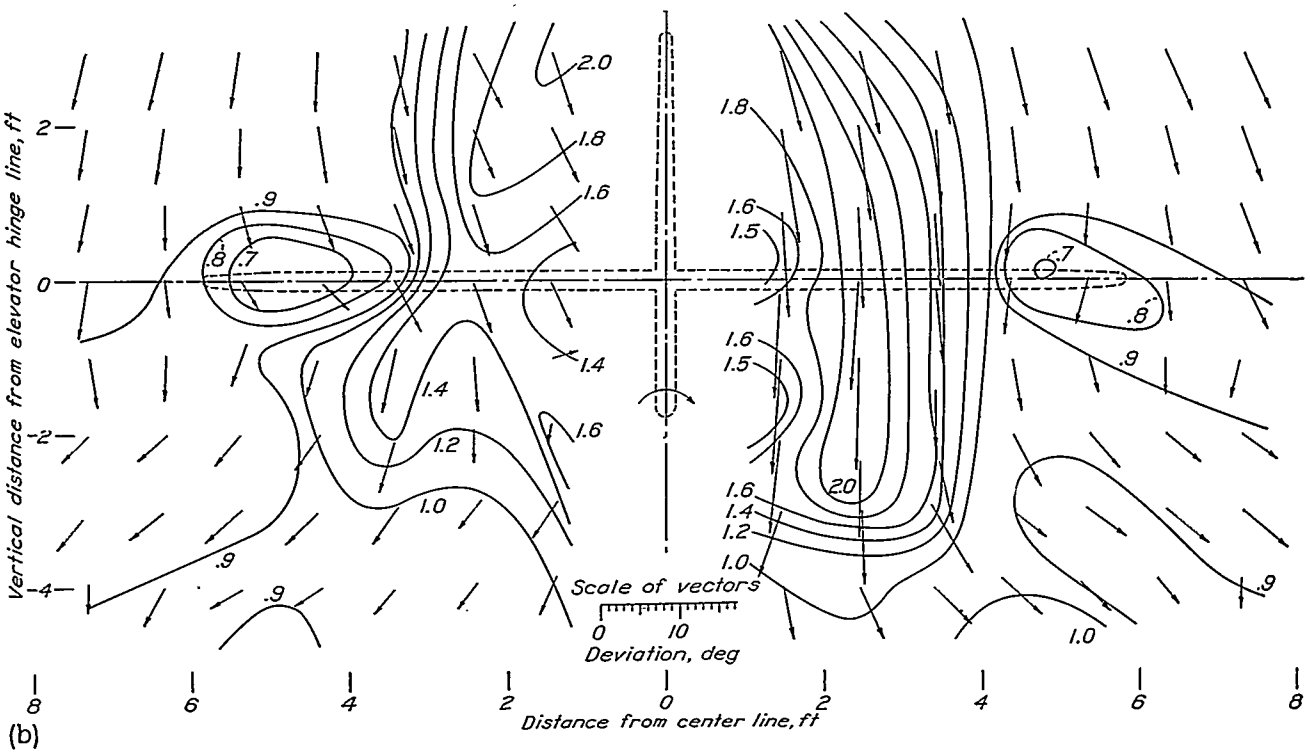

(b) Original condition; T_c', 0.194; T_c, 0.292; α, 13.7°.

FIGURE 22.

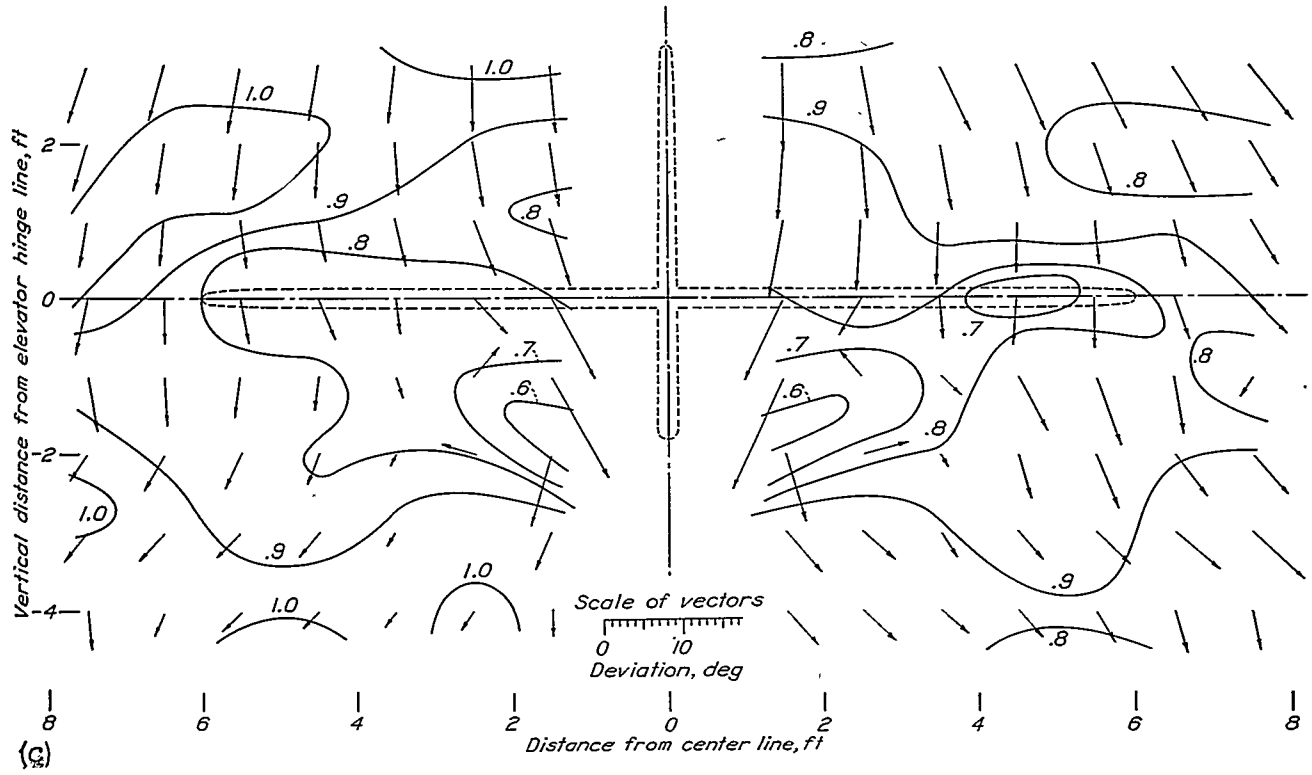

(c) With fillet and cowling; propeller removed; α, 13.7°.

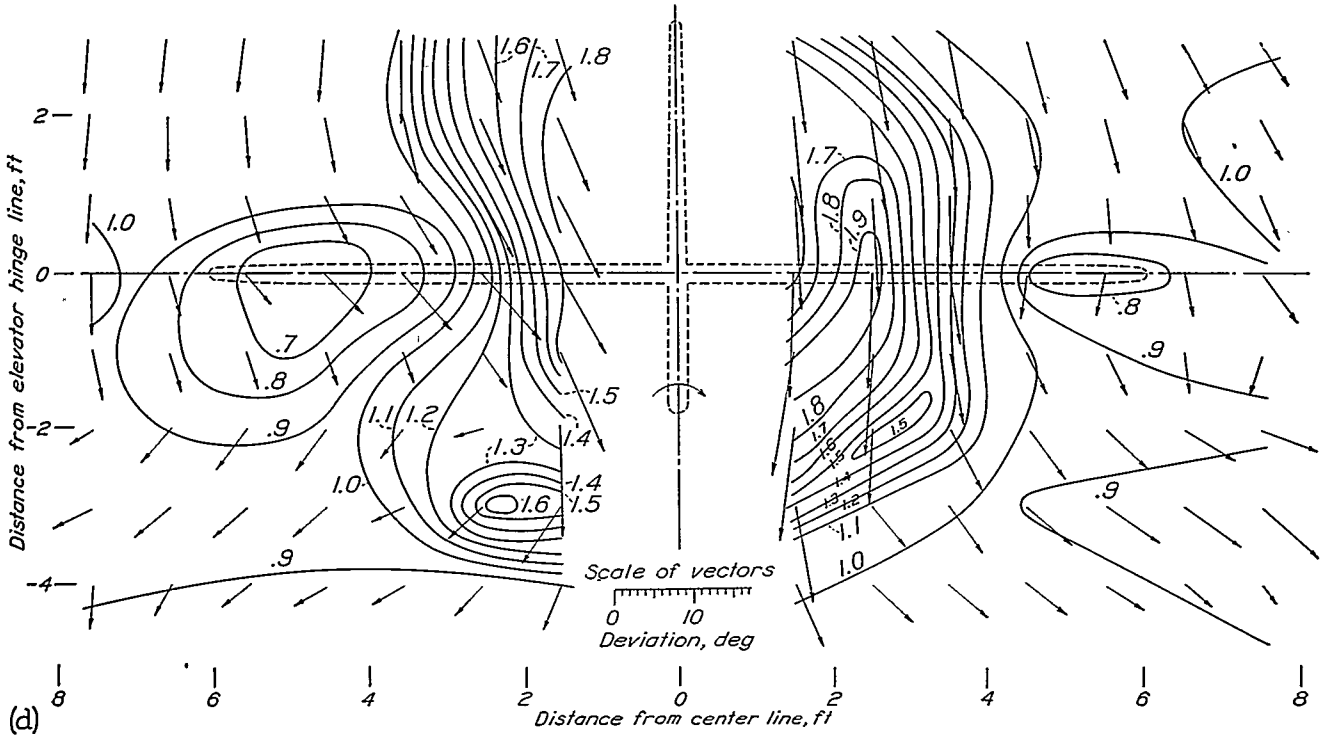

(d) With fillet and cowling; T_c', 0.165; T_c, 0.248; α, 13.7°.

FIGURE 22.—Dynamic-pressure (q/q_0) contours and inclination of the air stream in the plane of the elevator hinge line. Vectors show deviation of air flow from the free-stream direction. View looking forward. The McDonnell airplane.

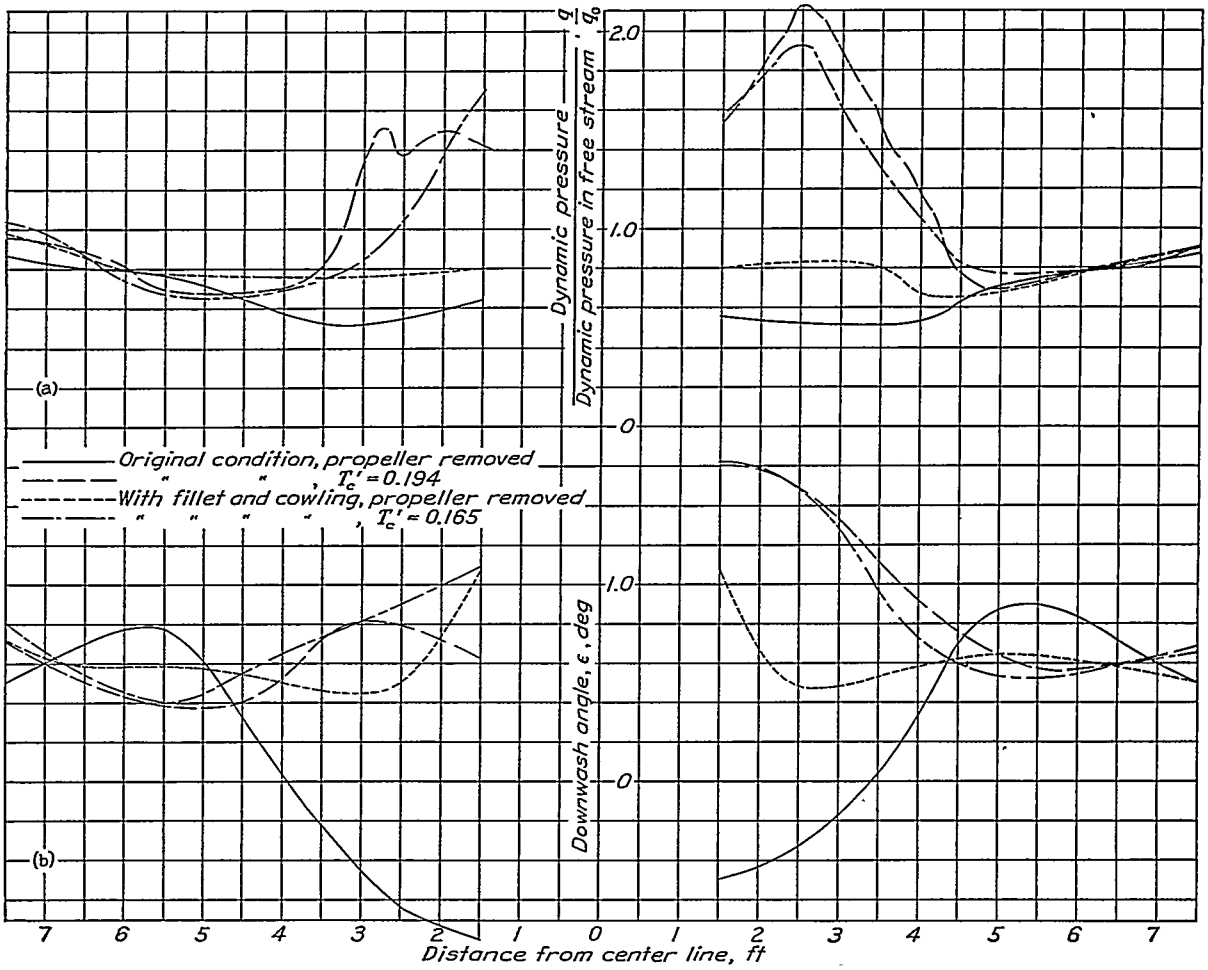

(a) Dynamic pressures across the elevator hinge line.
(b) Downwash angles across the elevator hinge line.

FIGURE 23.—Dynamic pressures and downwash angles for the McDonnell airplane. α, 14°, T_c=1.51 T_c'.

COMPARISON OF EFFECTIVE AND AVERAGE VALUES OF DYNAMIC PRESSURE AND DOWNWASH ANGLE AT THE TAIL FOR THE McDONNELL AIRPLANE

Condition	α (deg)	T_c' (a)	$(q/q_0)_{eff}$	$(q/q_0)_{av}$	ϵ_{eff} (deg)	ϵ_{av} (deg)
Original	14.2	0.194	0.48	0.69	−0.8	2.2
	13.7		.99	1.29	10.1	10.4
With fillet and cowling	13.9	.165	.81	.81	6.6	8.9
	13.7		.95	1.24	11.1	11.0

[a] Missing values indicate that the propeller was removed.

The agreement between the effective and the average dynamic pressures is best for the improved airplane with propeller removed and poorest for the original airplane with propeller removed. These two airplane conditions, it may be noted, also represent the two extremes in regularity of the air flow at the tail.

THE FOUR-ENGINE MODEL

A three-view drawing of the midwing four-engine tractor model is shown in figure 24. For the pusher-propeller arrangement, the nacelles were removed, the motors were placed within the wing, and the propellers (shown dotted) were driven through extension shafts. It will be seen that the model is of very clean design and the fuselage is relatively small. The same center-of-gravity position was used in computing pitching moments for both tractor and pusher arrangements. Measurements were made of the tractor and the pusher models for both propeller-removed and propeller-operating conditions.

The tail surface of this model passes through the fuselage. No corresponding area reduction is assumed, the lift

being considered to carry across the fuselage just as in the case of the main wing. Furthermore, the clearance between the elevator and the sides of the fuselage is small; accordingly, as for the flap on the main wing, the elevator should also be considered to carry across the fuselage. The corresponding tail areas are thus revised to: total horizontal tail, 32.7 square feet; elevator, 12.6 square feet. Since the nose of the elevator was rounded and fitted very snugly into the recessed trailing edge of the stabilizer, the value of $\frac{dC_{N_t}}{d\delta_e}\Big/\frac{dC_{N_t}}{d\delta_s}$ should be about 10 percent higher than the value indicated by figure 20 (references 7 and 8). Also, since the cut-out has been eliminated in this tail, the value of $dC_{N_t}/d\delta_s$ should be about 4 percent higher than the value indicated by figure 19. (See reference 7.)

The characteristics of the isolated tail surface are thus estimated to be

$$dC_{N_t}/d\delta_s=0.060$$
$$dC_{N_t}/d\delta_e=0.58\times 0.060=0.035$$

The aerodynamic center of the tail surface is assumed to be at the mean quarter-chord point, and the pitching-moment coefficient $C_{m_{(a.c.)_t}}$ is assumed equal to $-0.01\ \delta_e$. The vertical tail probably causes a reduction of not more than 1 percent in the effective tail area.

On the basis of these considerations, the control characteristics would be, if there were no interference effects on the air flow,

$$dC_m/d\delta_s=-0.0280$$
$$dC_m/d\delta_e=-0.0174$$

The four-engine tractor model.—In tests of the tractor model with the propellers removed, pitching-moment measurements at low angles of attack gave a value of $dC_m/d\delta_e$ of -0.0164. The value of $(q/q_0)_{eff}$ is thus 0.94. At higher angles of attack, the wake still further reduces the elevator effectiveness, as shown in the lowest curve of figure 25 (a). The effect of the slipstream on the tail effectiveness is also shown in the figure for values of T_c' up to 0.5. The detrimental effect of the wake at high angles of attack is eliminated by the slipstream even at the lowest thrust coefficient, probably because the slipstream prevents stalling of the flow over the wing. After this stalling has been eliminated, the elevator effectiveness increases approximately linearly with T_c', as indicated by the uniform separation of the curves.

The corresponding curves of $dC_m/d\delta_e$ against α for the model with flaps deflected 20°, as for take-off, are shown in figure 25 (b). Comparison with figure 25 (a) shows that the effect of the slipstream on the tail effectiveness is considerably less than for the case of flaps up and the contribution due to the slipstream approaches zero at an angle of attack of about −5°. The main effect of the flap thus appears to be a lowering of the slipstream, due to the increased downwash, so that, at an angle of attack of about −5°, the tail is just above the slipstream and, even at higher angles of attack, the tail is not deeply immersed in the slipstream. The flap probably also increases the distortion of the slipstream, thus further contributing to the low value of $dC_m/d\delta_e$.

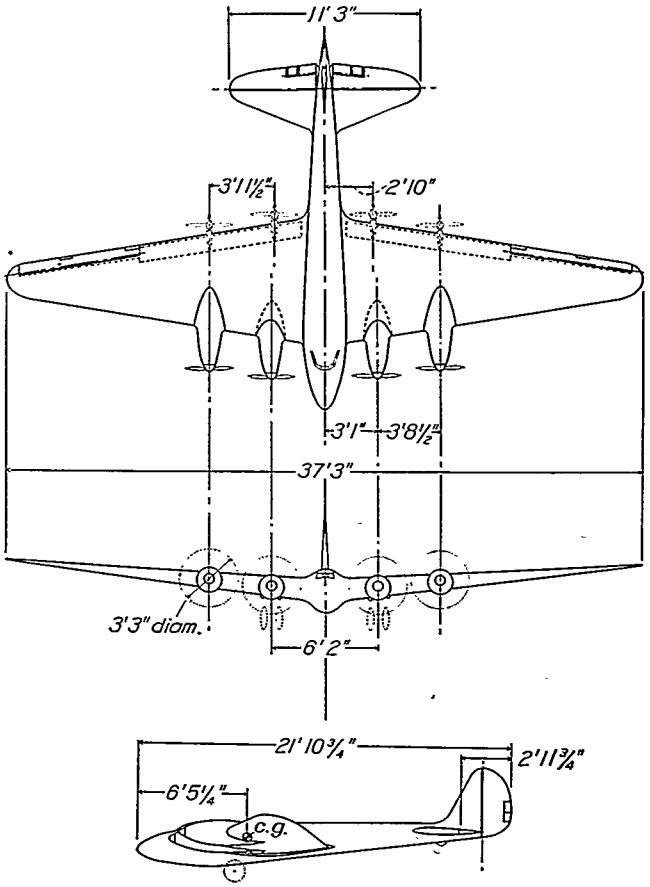

FIGURE 24.—Three-view drawing of the four-engine airplane model. Pusher propellers shown dotted. Areas, in square feet: wing, 172; horizontal tail, 31.4; elevator, 11.3.

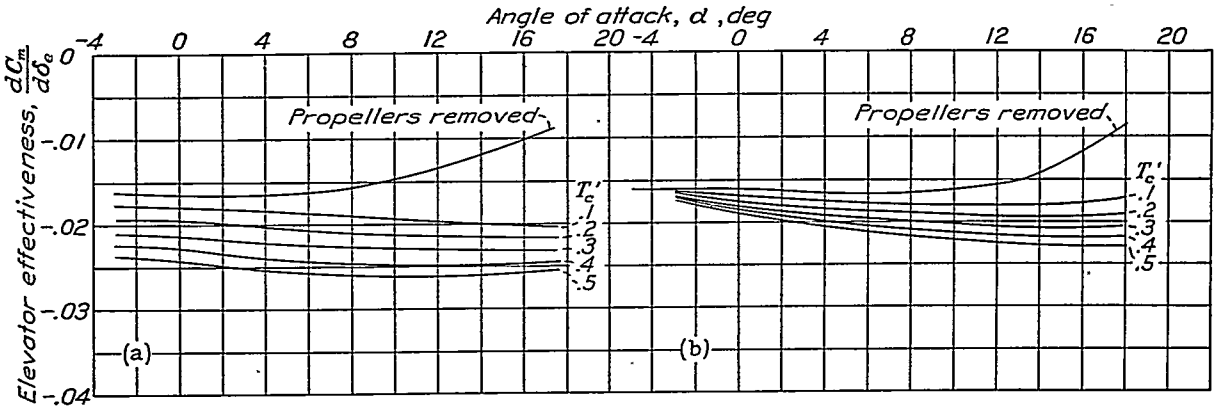

(a) δ_f=0°. (b) δ_f=20°.

FIGURE 25.—Elevator effectiveness for different power conditions. The four-engine tractor model; T_c=2.04 T_c'.

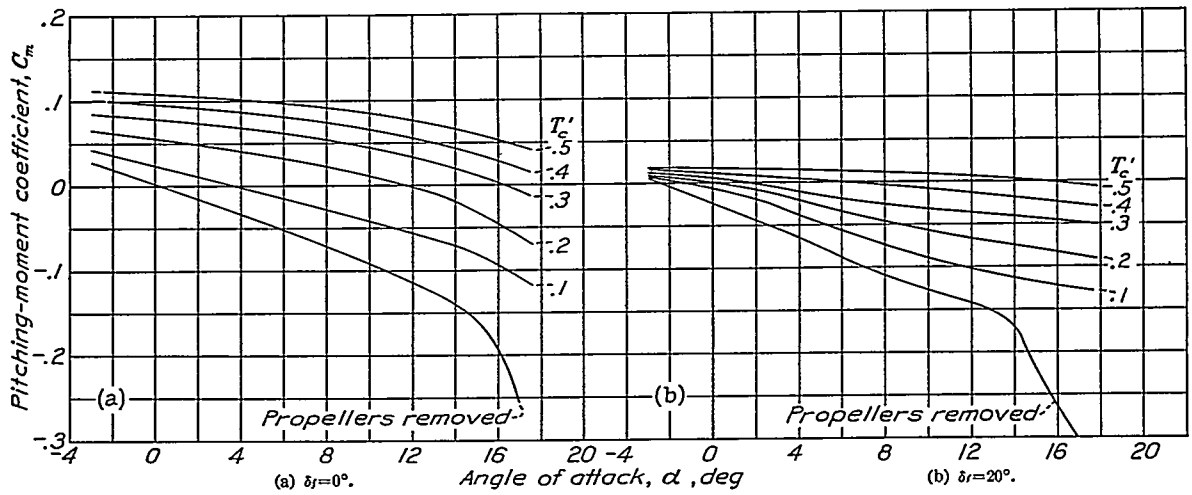

(a) δ_f=0°. (b) δ_f=20°.

FIGURE 26.—Effect of propeller operation on the pitching-moment coefficient. The four-engine tractor model; landing gear extended; δ_s, 0°; δ_e, 0°; T_c=2.04 T_c'.

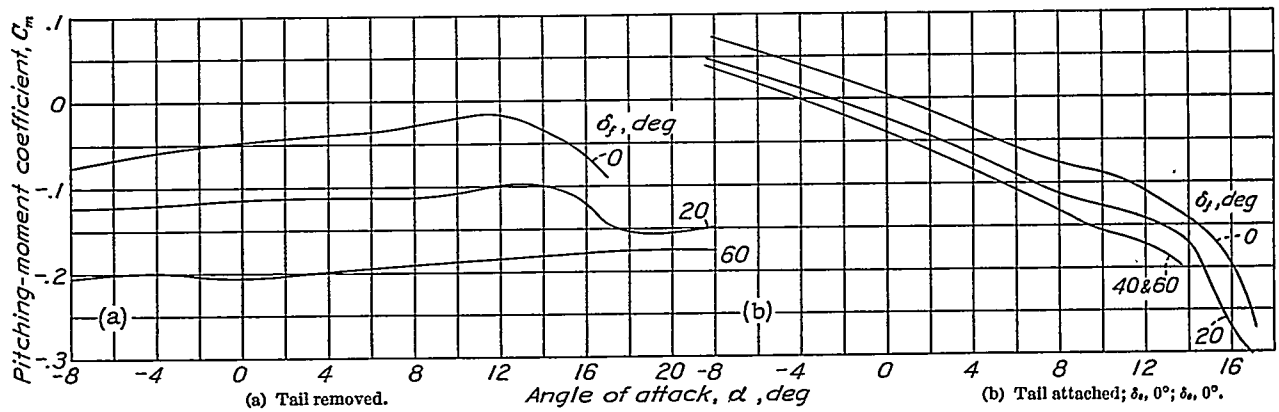

(a) Tail removed. (b) Tail attached; δ_s, 0°; δ_e, 0°.

FIGURE 27.—Effect of flap deflection on the pitching-moment coefficient. The four-engine tractor model; propellers removed.

The effect of propeller operation on stability, as determined by the slope of the pitching-moment curve, is shown in figure 26. The slope progressively decreases with increase in thrust. The curves also serve to show the effect of propeller operation on balance.

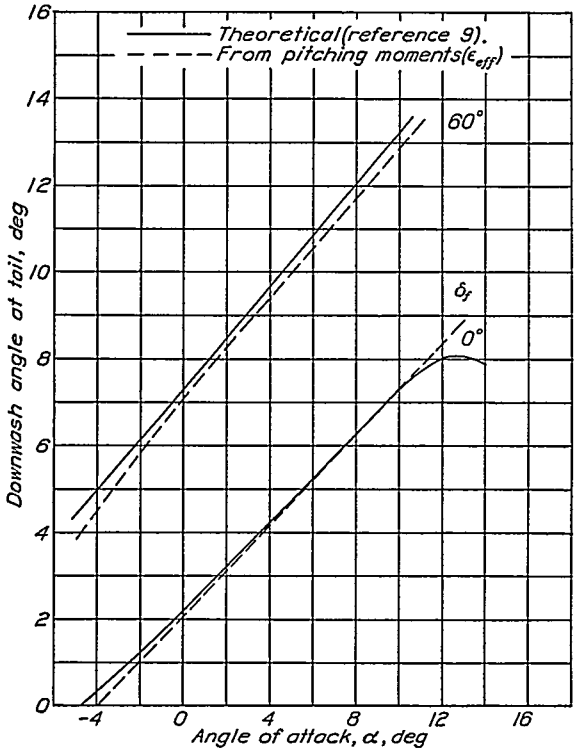

FIGURE 28.—Comparison of theoretical and experimental downwash angles. The four-engine tractor model; propellers removed.

Figure 26 (a) thus shows that, for $T_c'=0.1$, the airplane trims at $\alpha=3.8°$ and that increasing T_c' to 0.2 changes the angle of trim to 11.7°. This behavior, which is

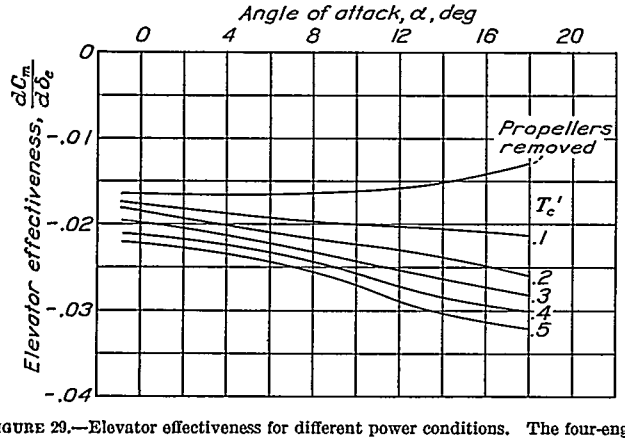

FIGURE 29.—Elevator effectiveness for different power conditions. The four-engine pusher model; $T_c=2.04\ T_c'$.

characteristic of most airplanes, is due to the increase of downwash with thrust.

The effects of flap deflection on the pitching moment for the propeller-removed condition are shown in figure 27. Figure 27 (a), for the tail removed, shows the large diving moment contributed by the flap. Figure 27 (b), for the complete airplane, shows that the increased downwash due to the flap increases the downward force on the tail nearly enough to neutralize the diving moment due to the flap.

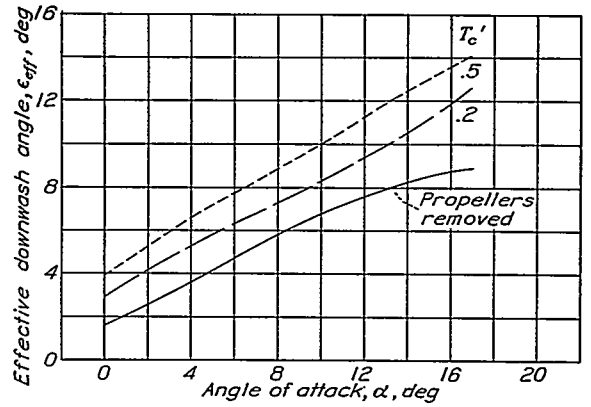

FIGURE 30.—Effect of propeller operation on the effective downwash angle at the tail. The four-engine pusher model; $T_c=2.04\ T_c'$.

The effective downwash angles, ϵ_{eff}, found from pitching-moment measurements, are plotted in figure 28

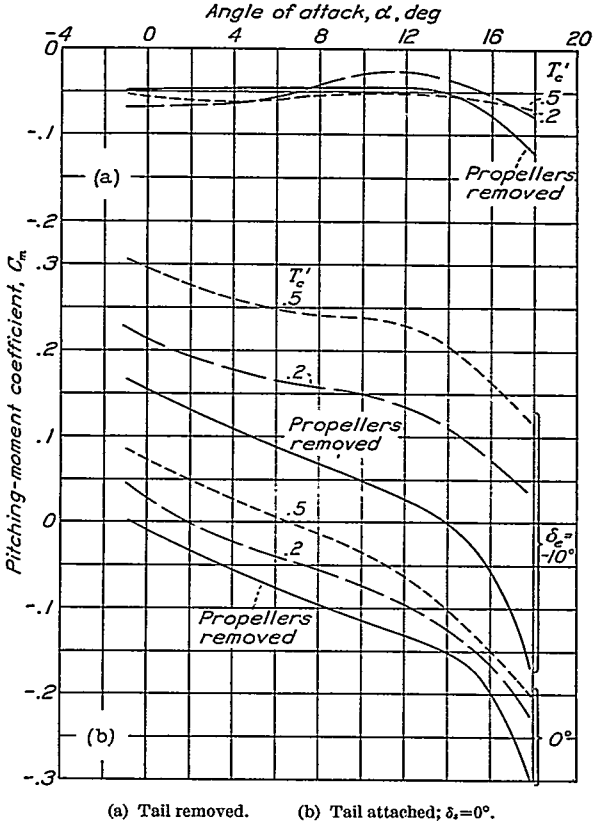

(a) Tail removed. (b) Tail attached; $\delta_e=0°$.

FIGURE 31.—Effect of propeller operation on the pitching-moment coefficient. The four-engine pusher model; $T_c=2.04\ T_c'$.

against angle of attack for the propeller-removed condition and with flaps neutral and deflected 60°. The downwash angles as predicted by the methods of reference 9 are also plotted and are in good agreement with the experimental values.

The four-engine pusher model.—The elevator effectiveness for the pusher model is plotted against angle of attack for different power conditions in figure 29. The slipstream effect is somewhat different from that for the tractor model. In particular, the increase in $dC_m/d\delta_e$ is less at low angles of attack and more at high angles, the variation being due to the fact that the tail advances into the slipstream with increasing angle of attack. That such an effect should occur is obvious from the relative positions of the propellers and the tail. The effect is much less definite in the case of the tractor model, owing to the distortion of the slipstream as it passes over the wing.

The effect of propeller operation on the effective downwash angle is shown in figure 30.

Pitching-moment coefficients are shown in figure 31 (a) for the model with the tail removed and, in figure 31 (b), for the model with the tail attached and two different elevator angles. The effect of the slipstream on longitudinal stability, as indicated by the slope of the pitching-moment curve, appears to be dependent

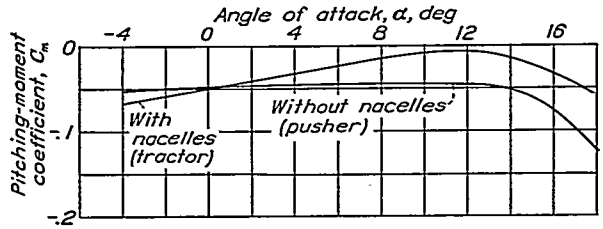

FIGURE 32.—Effect of nacelles on the pitching-moment coefficient. Comparison of the four-engine pusher and tractor models; propellers removed; tail removed.

on the elevator angle. Thus, the curves for $\delta_e=-10°$ show the usual decrease in stability with increase in thrust although the curves for $\delta_e=0°$ do not. Two different effects are involved: that of the slipstream in increasing the rate of increase of downwash angle with angle of attack; and the greater immersion of the tail in the slipstream at the higher angles, with correspondingly higher dynamic pressure at the tail. The effects are balanced for $\delta_e=0°$; therefore no change in the slope of the pitching-moment curve results. The second effect hardly exists in the case of the tractor model, the tail seeming to be immersed the same amount in the slipstream over the entire range of angles of attack.

The nacelles on the tractor model apparently affect the pitching moment. The effect can be seen in figure 32, in which the tail-removed pitching-moment curves for the pusher and the tractor models are compared. The nacelles considerably reduce the stability, corresponding to a forward movement of the aerodynamic center of about 5 percent of the mean chord.

Surveys of the air flow in the plane of the elevator hinge line for the pusher model are shown in figure 33. These surveys were made only on the right side although the air flow on the left side, for the propeller-operating condition, is different because all the propellers rotate in the same direction. The slipstreams appear to be somewhat deformed, as if the upper part were displaced inboard and the lower part outboard. This deformation can be ascribed to the influence of the trailing vortex sheet, which causes an inboard motion above it and an outboard motion below it. The effect is more pronounced at the higher angle of attack than at the lower (cf. figs. 33 (b) and 33 (d)), because the trailing vortex sheet is stronger. It is also more pronounced for the outboard than for the inboard slipstream, because the vortex sheet increases in strength toward the outer edge.

The measured dynamic pressures and the downwash angles over the right half of the elevator hinge line are plotted in figure 34. In the following table, the values of $(q/q_0)_{eff}$ and of ϵ_{eff} are compared with the average values as determined from the surveys over the right half of the hinge line. As before, the increase in $(q/q_0)_{eff}$ due to the slipstream is much less than the relative increase in average dynamic pressure.

COMPARISON OF EFFECTIVE AND AVERAGE VALUES OF DYNAMIC PRESSURE AND DOWNWASH ANGLE AT THE TAIL FOR THE FOUR-ENGINE PUSHER MODEL

α (deg)	T_c' [a]	$(q/q_0)_{eff}$	$(q/q_0)_{av}$	ϵ_{eff} (deg)	ϵ_{av} (deg)
−1.8	----------	0.94	1.00	1.0	1.1
−1.9	0.180	1.03	1.80	1.8	−.3
4.2	----------	.94	.91	3.8	5.1
4.1	.183	1.06	1.85	5.3	6.2
10.2	----------	.92	.81	6.8	6.7
10.2	.205	1.16	1.68	8.2	8.2

[a] Missing values indicate that the propeller was removed.

THE TWO-ENGINE PUSHER MODEL

A three-view drawing of the two-engine pusher model is shown in figure 35. The model was tested with the propellers removed and operating, with the flaps retracted and deflected, and with and without the horizontal tail.

The characteristics of the isolated tail surface are estimated to be

$$dC_N/d\delta_s=0.056$$
$$dC_N/d\delta_e=0.60\times dC_N/d\delta_s=0.034$$

The tail surface passes through the top of the fuselage and the vertical tail is placed somewhat back of the horizontal tail. As in the case of the four-engine model, this method of attachment probably reduces the tail effectiveness not over 1 percent. If the tail force is assumed to be applied at the mean quarter-chord position and if $C_{m(a.c.)_t}$ is assumed to be $-0.01\ \delta_e$, it follows that the control factors should be, except for the effect of the wake,

$$dC_m/d\delta_s=-0.0218$$
$$dC_m/d\delta_e=-0.0145$$

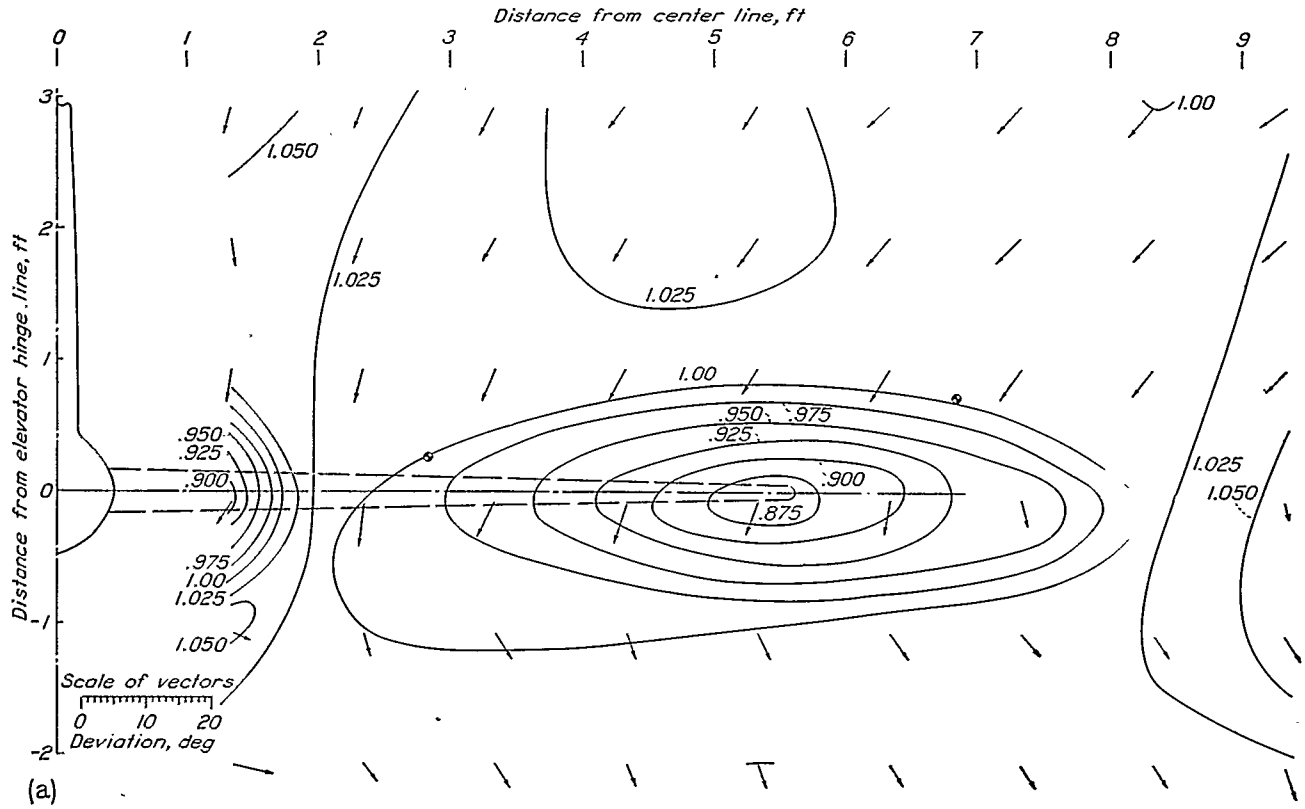

(a) Propellers removed; α, 4.2°.

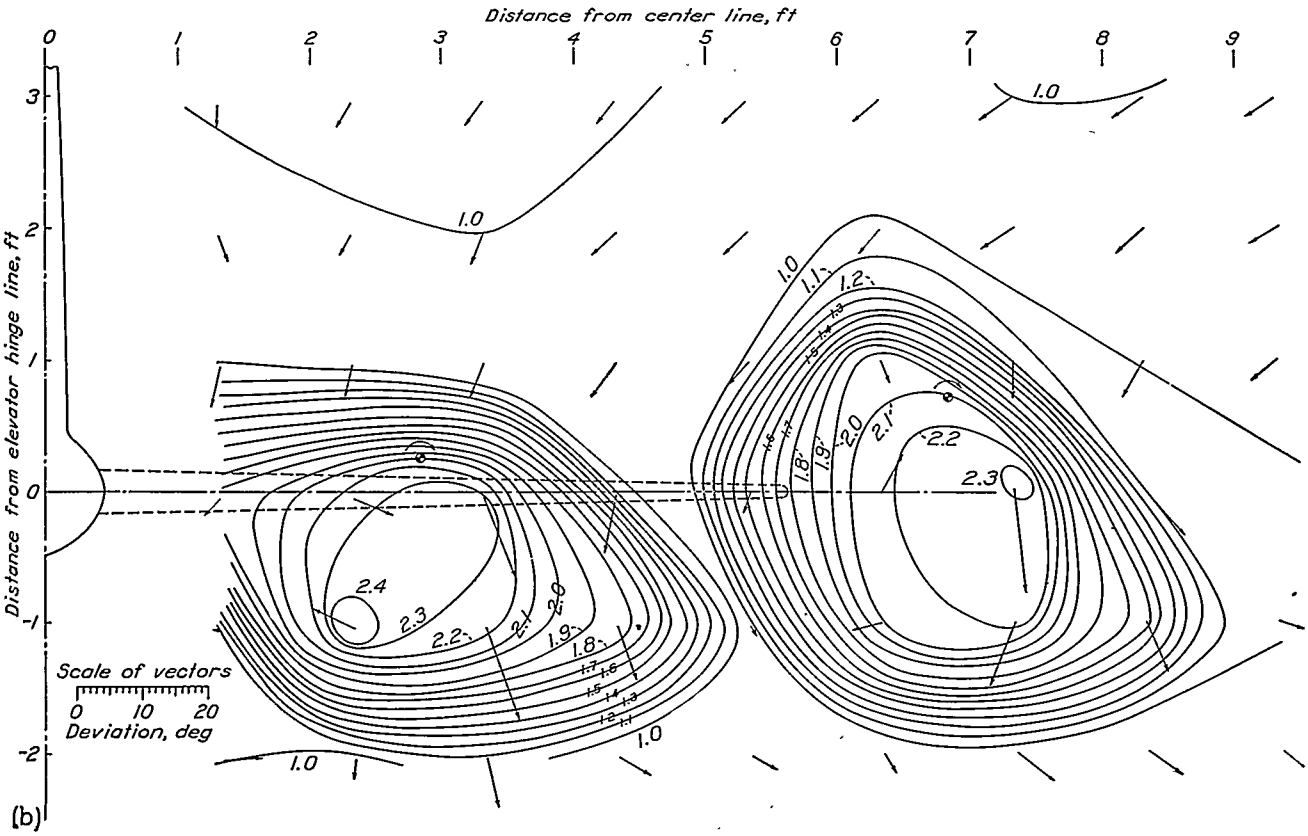

(b) V/nD, 0.489; T_c', 0.183; T_c, 0.373; α, 4.1°.

FIGURE 33.

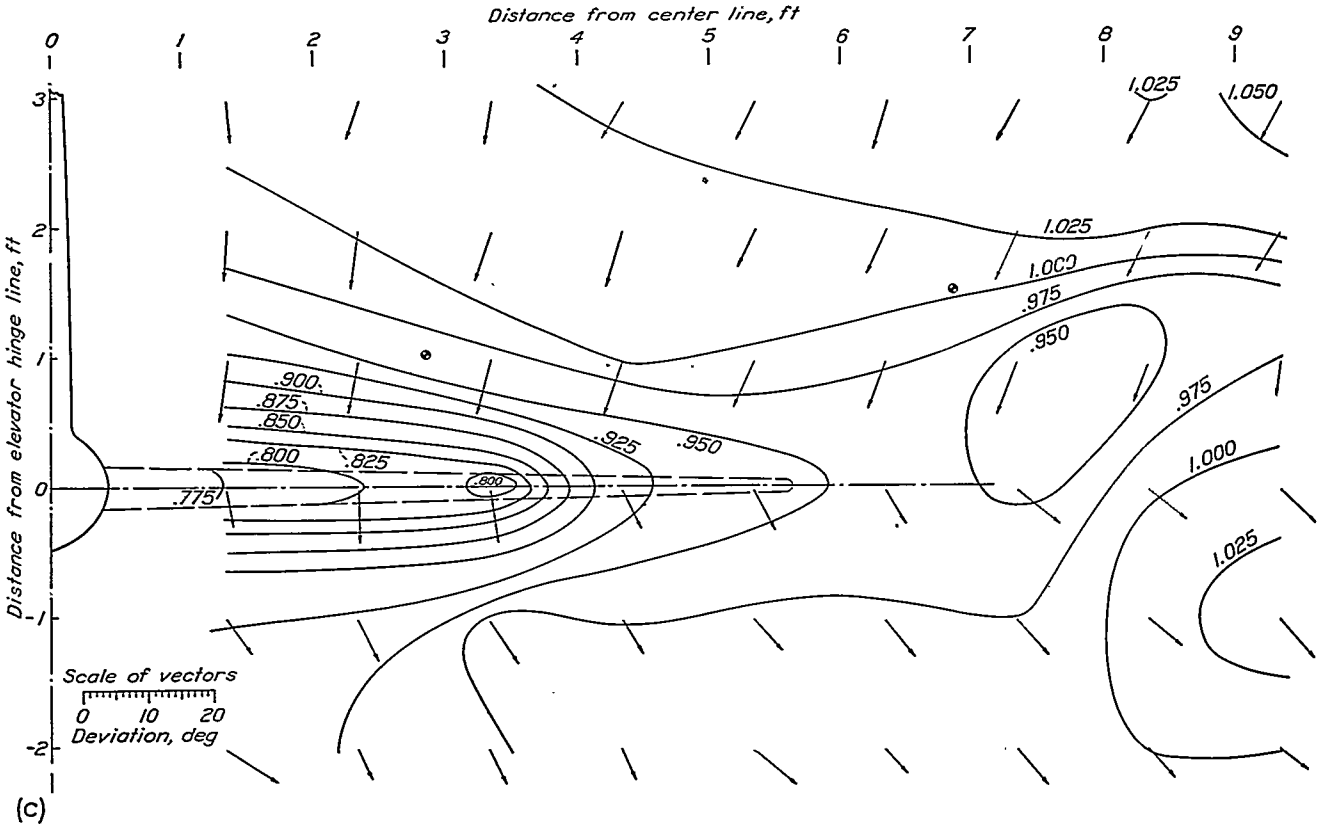

(c) Propellers removed; α, 10.2°.

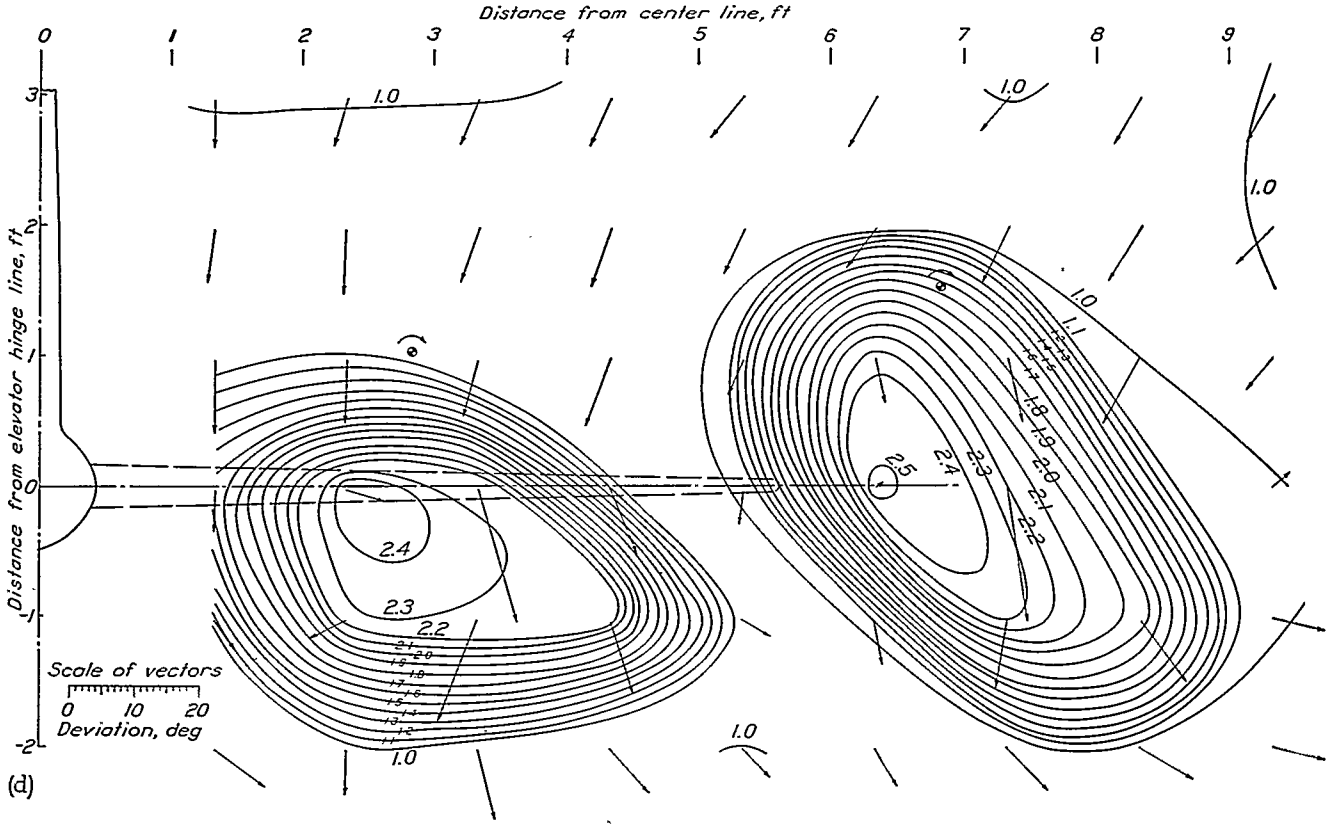

(d) V/nD, 0.470; T_c', 0.205; T_c, 0 418; α, 10.2°.

FIGURE 33.—Dynamic-pressure (q/q_0) contours and inclination of the air stream in the plane of the elevator hinge line. Vectors show deviation of air flow from free-stream direction. View looking forward. Circles show projections of propeller centers. The four-engine pusher model.

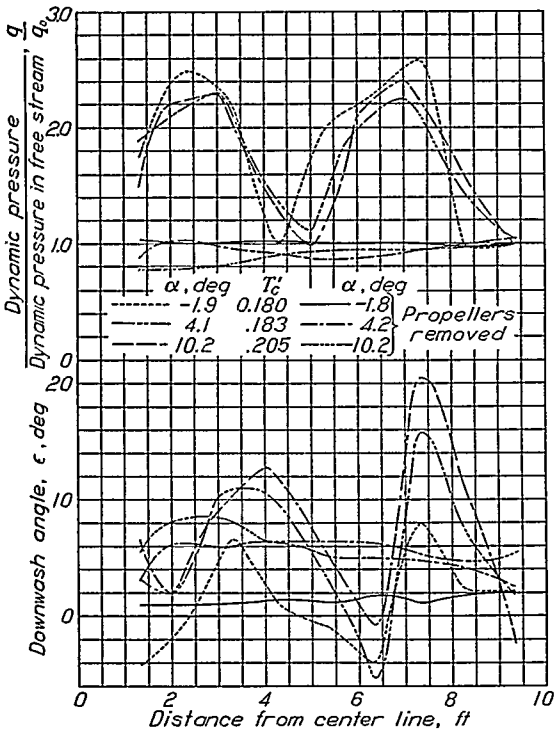

FIGURE 34.—Downwash angles and dynamic pressures across the elevator hinge line. The four-engine pusher model; $T_c=2.04\ T_c'$.

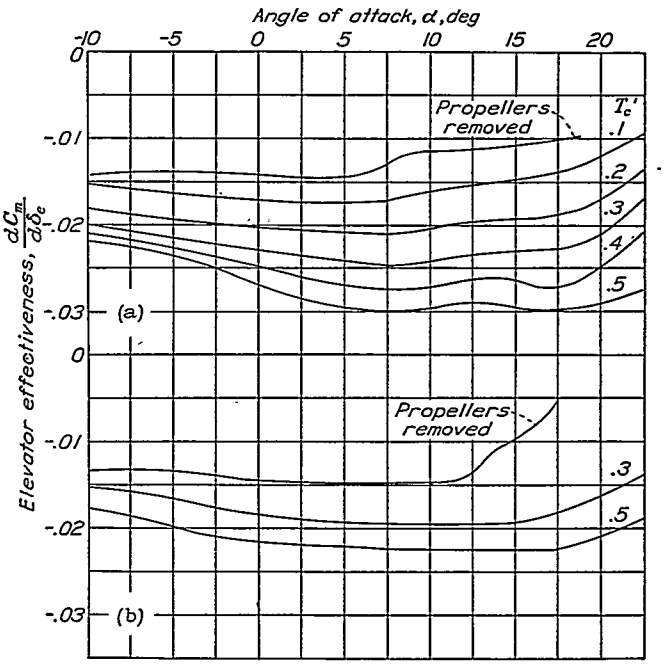

(a) Landing gear retracted; δ_f, 0°.
(b) Landing gear extended; δ_f, 45°.

FIGURE 36.—Elevator effectiveness for different power conditions. The two-engine pusher model; $T_c=1.30\ T_c'$.

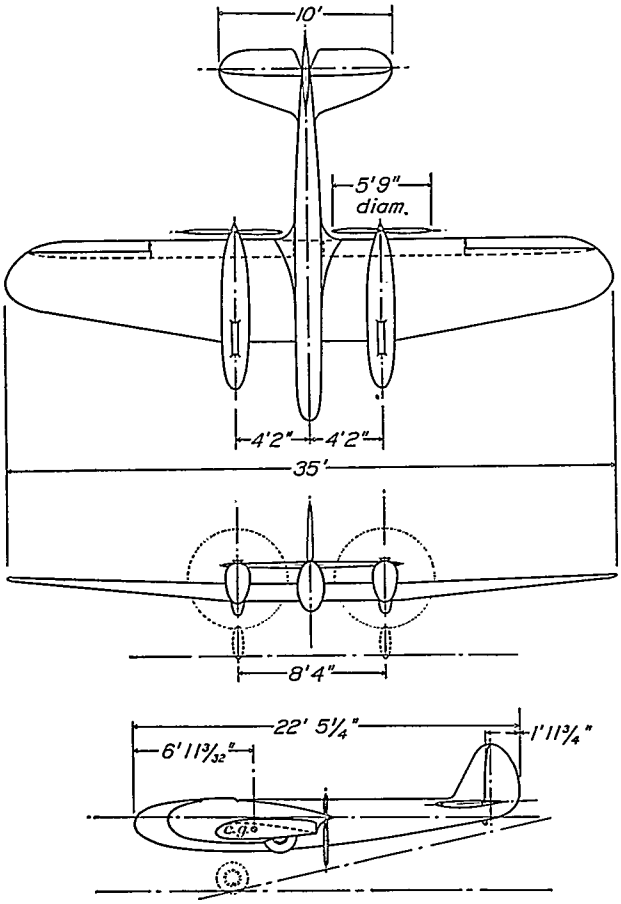

FIGURE 35.—Three-view drawing of the two-engine pusher model. Areas, in square feet: wing, 172; horizontal tail, 28.2; gross elevator, 12.4; elevator back of hinge, 9.2.

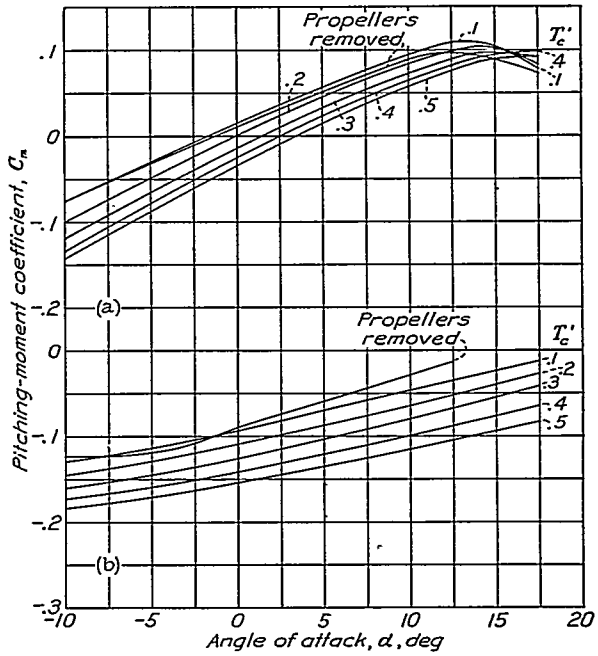

(a) Landing gear retracted; δ_f, 0°.
(b) Landing gear extended; δ_f, 45°.

FIGURE 37.—Effect of propeller operation on the pitching-moment coefficient. The two-engine pusher model; tail removed; $T_c=1.30T_c'$.

No experimental value of $dC_m/d\delta_s$ was available for comparison. With propellers removed, the highest experimental value of $dC_m/d\delta_e$ was -0.0145, which is equal to the value just mentioned. There thus appears to be no interference at all $[(q/q_0)_{eff}=1.00]$ on the air flow over the tail surface at low angles of attack, a result that may appear incredible. The tail, however, is obviously well above the wing wake; and the air-flow surveys, as will subsequently appear, also showed no reduction in dynamic pressure at the tail.

In figure 36, $dC_m/d\delta_e$ is plotted against angle of attack for flap deflections of 0° and 45° and for various thrust coefficients. With the propellers removed, the tail is in the wing wake at high angles of attack and the tail

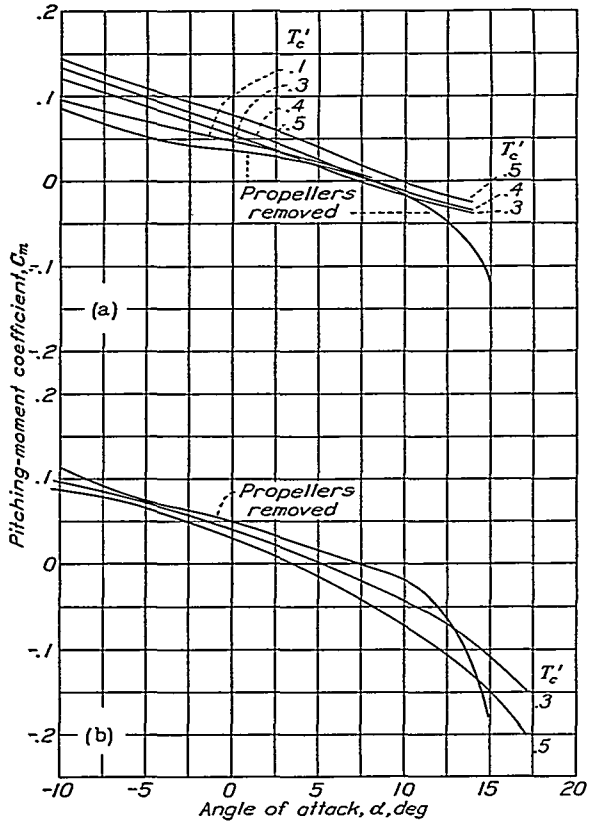

(a) Landing gear retracted; δ_f, 0°.
(b) Landing gear extended; δ_f, 45°.

FIGURE 38.—Effect of propeller operation on the pitching-moment coefficient. The two-engine pusher model; δ_s, 1.5°; δ_e, 0°; $T_c=1.30\ T_c'$.

effectiveness is correspondingly reduced. It is interesting to note that this reduction occurs at a higher angle of attack when the flaps are deflected than when they are retracted, which is explained by the fact that the stronger downwash when the flaps are deflected carries the wake down so that the tail enters it at the higher angle. The same effect may be noted for the four-engine model. (Cf. fig. 25.)

The effect of thrust on the elevator effectiveness is somewhat more pronounced than for any of the airplanes yet discussed. Deflecting the flap reduces the effect, as in the case of the four-engine model, because the increased downwash depresses the slipstream so that only the upper edge passes over the tail.

The pitching-moment coefficients for the tail-removed condition are plotted against angle of attack for various values of T_c' in figure 37. Since the thrust line is above the center of gravity, the thrust causes a diving moment. Lowering the flap increases the effect, for the diving moment contributed by the flap also increases with the thrust. Pitching-moment coefficients for the tail-on condition are plotted in figure 38. Because the increased downwash due to the slipstream and the diving moment due to the high thrust line have opposite effects, the effect of propeller operation on balance is less for this airplane than for the other airplanes studied.

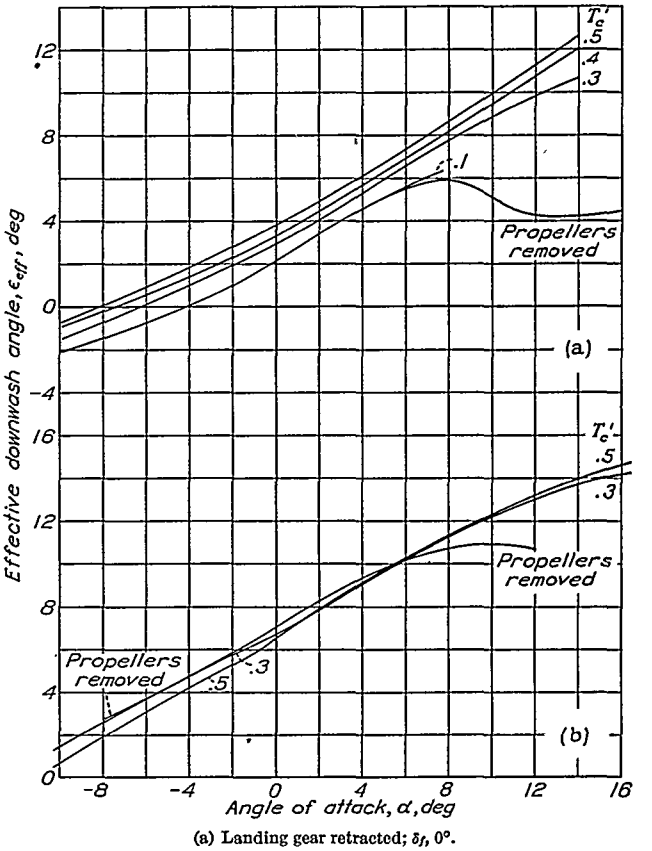

(a) Landing gear retracted; δ_f, 0°.
(b) Landing gear extended; δ_f, 45°.

FIGURE 39.—Effect of propeller operation on the effective downwash angle at the tail. The two-engine pusher model; $T_c=1.30\ T_c'$.

By a comparison of the pitching-moment coefficients for the tail-on and the tail-removed conditions, effective downwash angles were computed, which are plotted in figure 39 against angle of attack. The value of the stabilizer setting was somewhat uncertain, so the actual values are probably not correct; the inaccuracy, however, does not apply to the differences between the curves.

Some surveys of the air flow in the plane of the elevator hinge line (on only the right side) are shown in figure 40. For the propeller-removed condition, it will be seen that the wake, for $\alpha=7.8°$, is mainly below

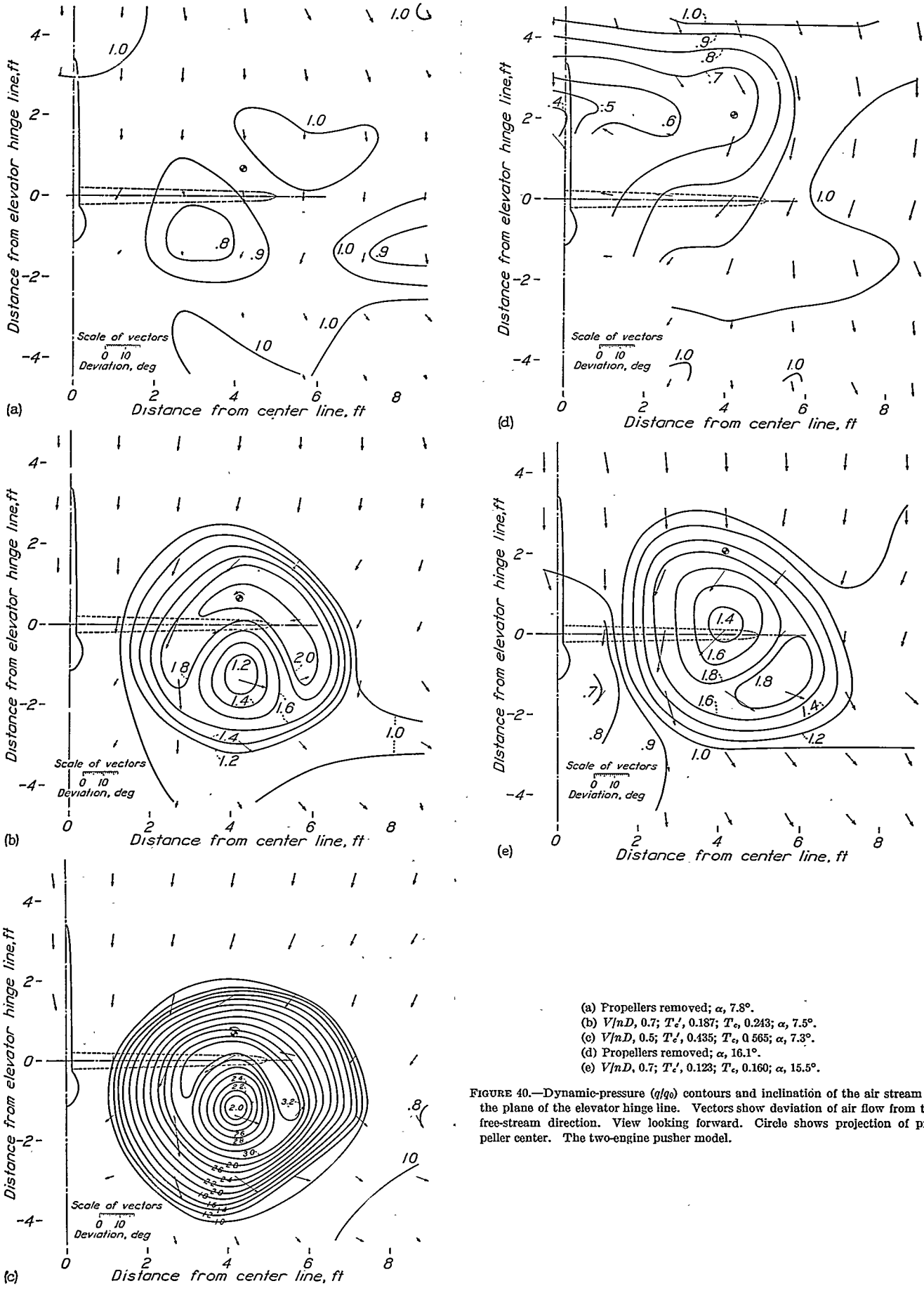

(a) Propellers removed; α, 7.8°.
(b) V/nD, 0.7; T_c', 0.187; T_c, 0.243; α, 7.5°.
(c) V/nD, 0.5; T_c', 0.435; T_c, 0.565; α, 7.3°.
(d) Propellers removed; α, 16.1°.
(e) V/nD, 0.7; T_c', 0.123; T_c, 0.160; α, 15.5°.

FIGURE 40.—Dynamic-pressure (q/q_0) contours and inclination of the air stream in the plane of the elevator hinge line. Vectors show deviation of air flow from the free-stream direction. View looking forward. Circle shows projection of propeller center. The two-engine pusher model.

the tail but that, for the stalled condition (α=16.1°), it is mainly above the tail. In figure 41 are plotted the relative dynamic pressures and the downwash angles across the elevator hinge line, as found from these and other surveys.

In the following table, $(q/q_0)_{eff}$ and ϵ_{eff}, as determined from pitching moments, are compared with the average values found from the surveys. The agreement between $(q/q_0)_{eff}$ and $(q/q_0)_{av}$ is much closer than for any of the previous three airplanes.

of the same air is given by the integral $2\int qr\theta dS$, where

dS an element of area of the slipstream cross section.

r the distance to a convenient center of rotation (chosen near the middle of the slipstream).

θ the angle, in radians, between the direction of the air flow and the plane perpendicular to the survey plane, passing through the chosen center and the variable point.

These integrals were evaluated for the six propeller-operating surveys, corrections being made for the propeller-removed air flow in the same region. The agreement between the thrust and the first integral was satisfactory, but the measured engine torque was generally about 25 percent lower than the value given by the second integral. The results were sufficiently consistent to indicate that the distributions of dynamic pressure and of angular velocity in the slipstream behind pusher propellers can probably be correlated with the values of the thrust and the torque.

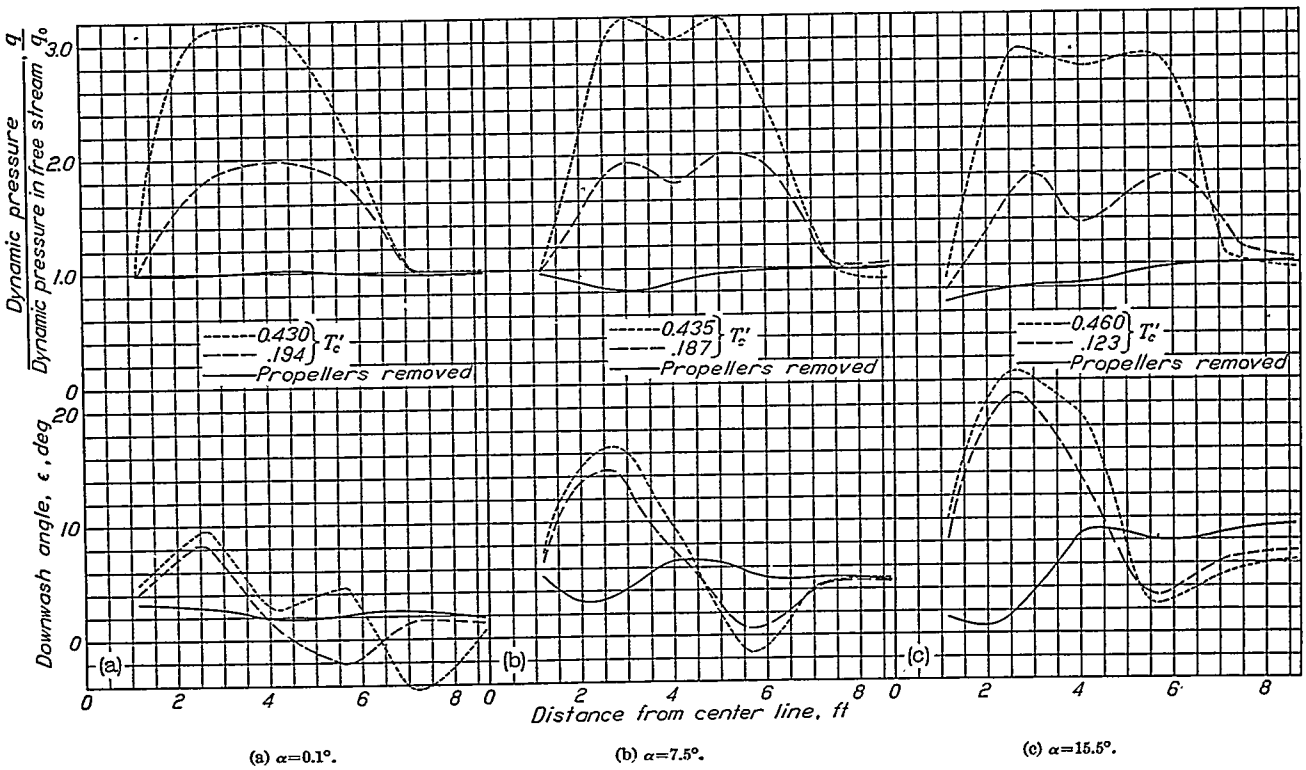

(a) α=0.1°. (b) α=7.5°. (c) α=15.5°.

FIGURE 41.—Downwash angles and dynamic pressures across the elevator hinge line. The two-engine pusher model; T_c=1.30 T_c'.

COMPARISON OF EFFECTIVE AND AVERAGE VALUES OF DYNAMIC PRESSURE AND DOWNWASH ANGLE AT THE TAIL FOR THE TWO-ENGINE PUSHER MODEL

α (deg)	T_c' [a]	$(q/q_0)_{eff}$	$(q/q_0)_{av}$	ϵ_{eff} (deg)	ϵ_{av} (deg)
0.2	----------	0.96	1.00	2.3	2.8
.1	0.430	1.78	2.33	3.7	6.8
.1	.194	1.27	1.48	2.6	4.9
7.8	----------	.88	.94	5.9	5.0
7.3	.435	1.97	2.08	8.0	12.5
7.5	.187	1.41	1.46	6.9	10.1
16.1	----------	.74	.77	4.5	3.3
15.5	.460	1.98	2.01	13.0	19.2
15.5	.123	1.11	1.20	8.0	15.7

[a] Missing values indicate that the propeller was removed.

Some computations were made to determine whether the linear and the angular velocities of the slipstreams corresponded, respectively, to the measured thrusts and engine torques. The increase in momentum experienced by the air in the part of the slipstream that passes through the survey plane per second is given by the integral $2\int q(1-\sqrt{q_0/q})dS$, and the angular momentum

THE SOC–1 AIRPLANE

A three-view drawing of the SOC–1 single-engine two-place biplane is shown in figure 42. This airplane has an automatic leading-edge slat and a trailing-edge plane flap, both on the upper wing. Propeller-removed and propeller-operating tests were made with the slat closed and the flap retracted and with the slat open and the flap deflected 40°. For this airplane, as for those

to be subsequently discussed, no experiments were made with the tail removed and no surveys were made of the air flow in the region of the tail.

In figure 43, the maximum values of $dC_m/d\delta_e$ are plotted against angle of attack for the two flap conditions and for various thrust coefficients. In figure 44, the pitching-moment coefficient is plotted against angle of attack for the same conditions and for $\delta_e=0°$. Propeller operation raises the pitching moment in both cases; it decreases stability for the slat-closed flap-retracted condition (for $\delta_e=0°$) and increases it for the slat-open flap-deflected condition.

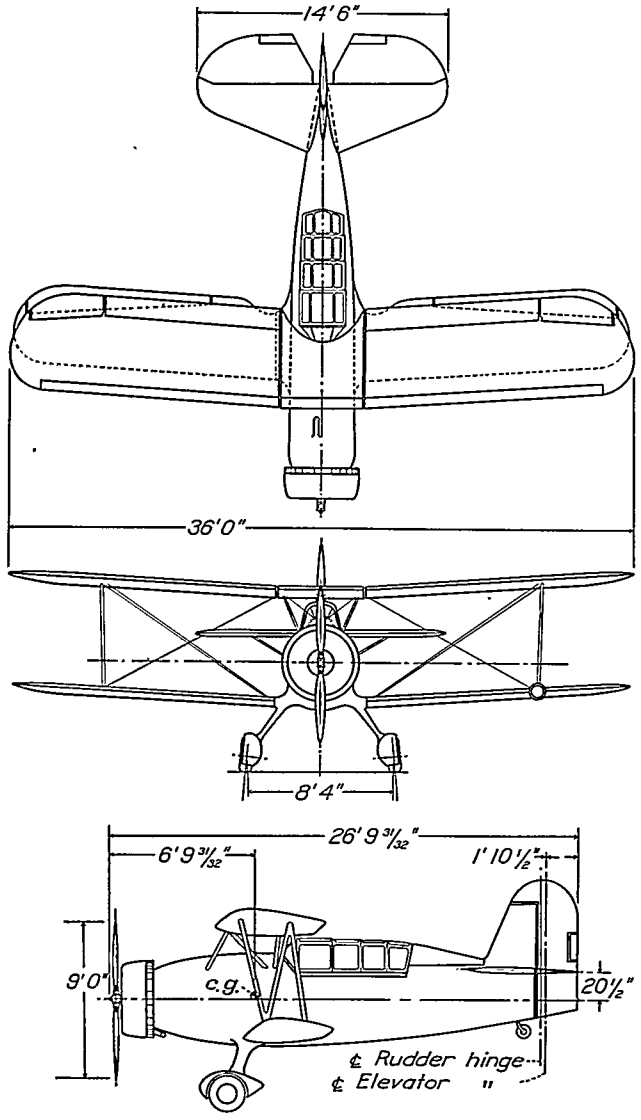

FIGURE 42.—Three-view drawing of the SOC-1 airplane. Areas, in square feet: wing, 348; horizontal tail, 70.7; gross elevator, 31.5; elevator back of hinge, 25.0.

The characteristics of the isolated tail surface are estimated to be

$$\frac{dC_{N_t}}{d\delta_s}=0.045$$

$$\frac{dC_{N_t}}{d\delta_e}=0.061\times\frac{dC_{N_t}}{d\delta_s}=0.0265$$

The vertical tail may be assumed to reduce the effective tail area by 1 percent. If $C_{m_{(a.c.)_t}}$ is assumed to be $-0.01\delta_e$, it follows that the control factor should be, except for the effect of the wake, $dC_m/d\delta_e=-0.0182$. The highest experimental value for the propeller-

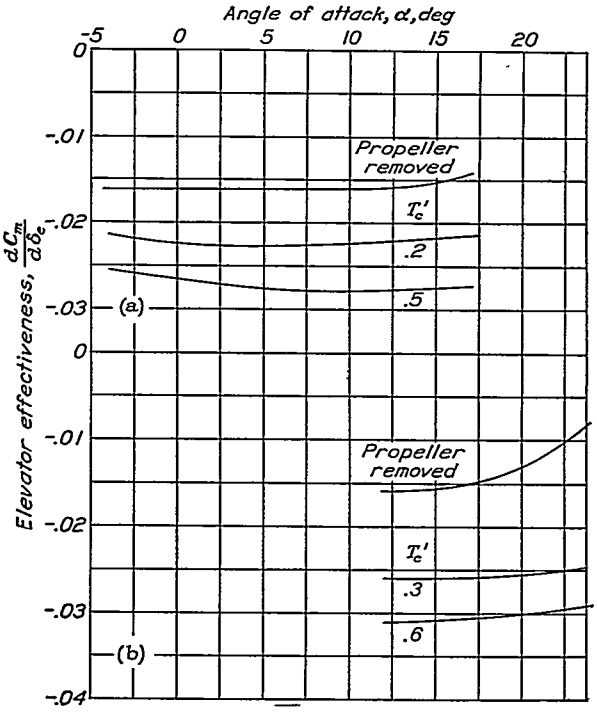

(a) Slat closed; δ_f, 0°.
(b) Slat open; δ_f, 40°.

FIGURE 43.—Elevator effectiveness for different power conditions. The SOC-1 airplane; $T_c=2.15\ T_c'$.

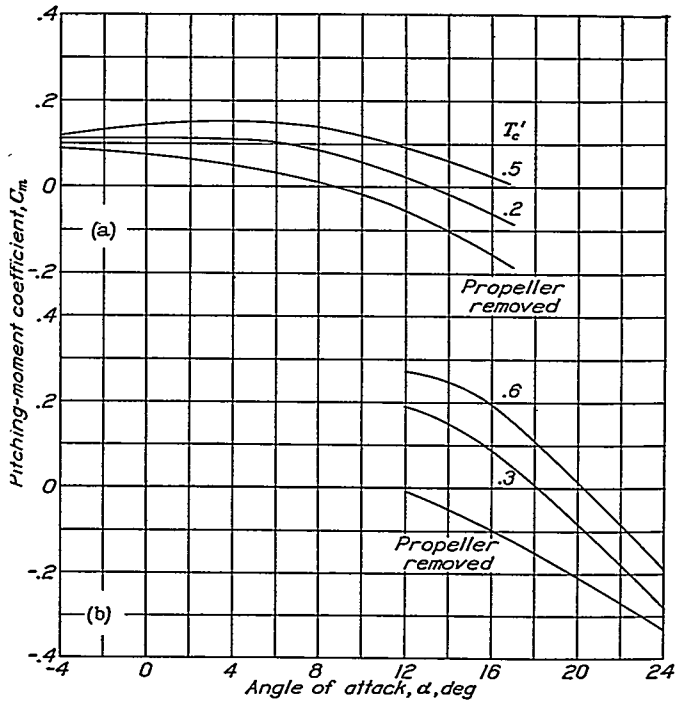

(a) Slat closed; δ_f, 0°.
(b) Slat open; δ_f, 40°.

FIGURE 44.—Effect of propeller operation on the pitching-moment coefficient. The SOC-1 airplane; δ_e, 0°; $T_c=2.15\ T_c'$.

removed condition was −0.0161, corresponding to $(q/q_0)_{eff}=0.89$.

THE XSBC–3 AIRPLANE

A three-view drawing is shown in figure 45 of the XSBC–3 single-engine two-place biplane. This airplane has a full-span plain flap on the lower wing. Tests were made with the propeller both removed and operating and with the flap retracted and deflected.

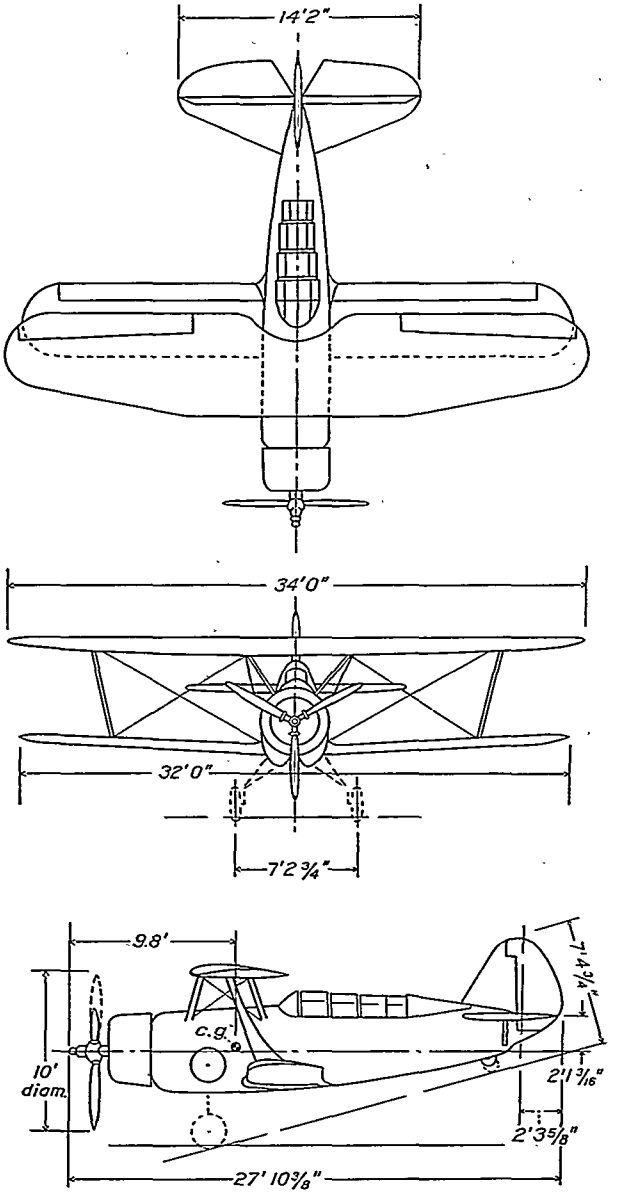

FIGURE 45.—Three-view drawing of the XSBC–3 airplane. Areas, in square feet: wing, 317; horizontal tail, 57.8; gross elevator, 29.4; elevator back of hinge, 23.4.

Figures 46 and 47 show the variation with angle of attack of elevator effectiveness and pitching-moment coefficient for the various flap and power conditions. The increment of elevator effectiveness due to power increases with angle of attack. The flap lowers the pitching-moment curve and also decreases the slope. Propeller operation increases the pitching-moment coefficient.

The characteristics of the isolated tail surface are estimated to be

$$\frac{dC_{N_t}}{d\delta_s}=0.053$$

$$\frac{dC_{N_t}}{d\delta_e}=0.68\times 0.053=0.036$$

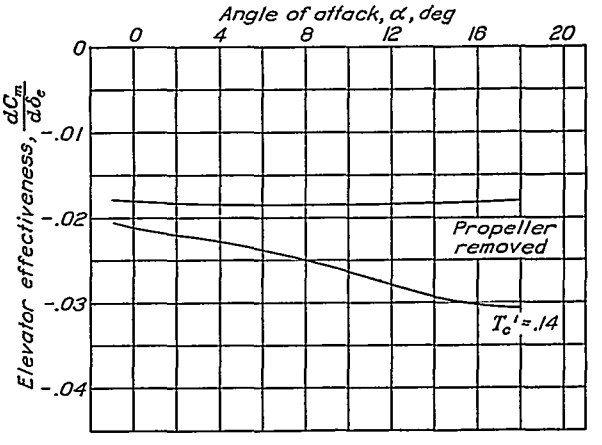

FIGURE 46.—Elevator effectiveness for propeller-removed and propeller-operating conditions. The XSBC-3 airplane; $T_c=1.59\ T_c'$.

If it is assumed that the vertical tail reduces the effective area by 1 percent, and if $C_{m_{(a.c.)_t}}$ is assumed to be $-0.01\ \delta_e$, the control factor should be, except for the effect of the wake, $dC_m/d\delta_e=-0.0210$. The highest experimental value for the propeller-removed condition was −0.0185, corresponding to $(q/q_0)_{eff}=0.88$.

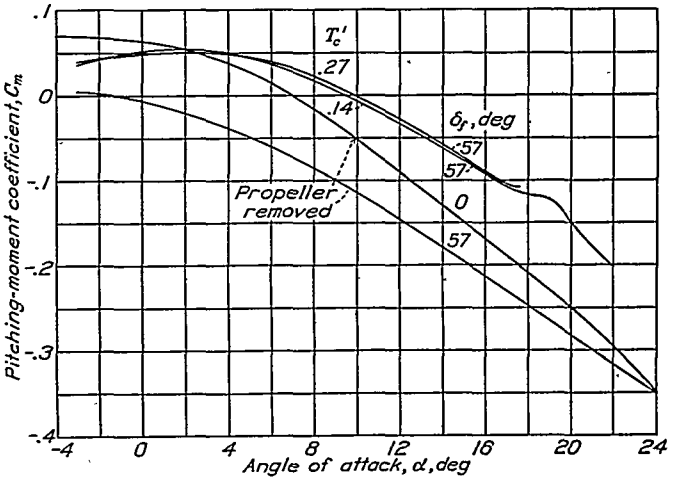

FIGURE 47.—Effect of flap deflection and propeller operation on the pitching-moment coefficient. The XSBC-3 airplane; δ_s, 0°; $T_c=1.59\ T_c'$.

THE XO4U–2 AND THE SB2U–1 AIRPLANES

Two of the airplanes for which elevator-effectiveness data were available were tested only with the propeller removed. The data were studied only with respect to the values of $dC_m/d\delta_e$.

The XO4U–2 single-engine two-place biplane is similar to the SOC–1 or the XSBC–3 and has a somewhat

similar tail arrangement. The value of $dC_m/d\delta_e$ was about −0.0145 over the range of angles below the stall, the corresponding value of $(q/q_0)_{eff}$ being 0.90.

The SB2U–1 single-engine low-wing monoplane was tested only with the landing flaps down. The value of $dC_m/d\delta_e$ was about −0.014, as compared with a value of −0.0157 computed for the free-stream dynamic pressure at the tail. The value of $(q/q_0)_{eff}$ for the low angles of attack is thus about 0.89.

CONCLUDING REMARKS

Following are summarized some of the results of general interest obtained from the study of data obtained in the full-scale wind tunnel:

1. The pitching-moment coefficient of a typical tail surface about its aerodynamic center was about −0.01 times the elevator angle. This value corresponds to about 6 or 8 percent of the elevator effectiveness of a complete airplane.

2. With propeller removed and at low angles of attack, the effective dynamic pressure at the tail q was nearly equal to the free-stream dynamic pressure q_0 $[(q/q_0)_{eff}=1.0]$ for the most favorable case; for a thick-fuselage biplane, the highest value of $(q/q_0)_{eff}$ was 0.88. The values decreased at higher angles of attack as the tail approached or entered the wing wake, the largest observed decrease, below the stall, being about 40 percent.

3. The loss in elevator effectiveness at high angles of attack, propeller removed, due to the wake from the wing roots or nacelles, was largely eliminated by operation of the propeller.

4. Propeller operation at thrust coefficients and angles of attack corresponding to high-speed flight increased $(q/q_0)_{eff}$ by about 2 to 4 percent. The highest observed increase at a thrust coefficient based on wing area T_c' equal to 0.5 and in the higher angle-of-attack range (corresponding to full-throttle landing or full-throttle climb for a high-powered airplane) was 110 percent for the two-engine pusher model.

5. The effective dynamic pressure was less than the average dynamic pressure at high thrust coefficients. In a typical example, with $T_c'=0.139$, $(q/q_0)_{eff}$ was only 1.30 when $(q/q_0)_{av}$ was 1.70.

6. At the higher thrust coefficients, $(q/q_0)_{eff}$ generally increased with angle of attack, probably because, for these airplanes, the tail was near the top of the slipstream at low angles of attack and advanced into it as the angle of attack increased.

7. The rate of increase of effective downwash angle ϵ_{eff} with angle of attack α, $d\epsilon_{eff}/d\alpha$, was considerably increased by propeller operation in the case of the gull-wing and the parasol-wing monoplanes, only slightly increased in the case of the four-engine pusher, and increased hardly at all in the case of the two-engine pusher. The downwash angle itself, however, was increased by propeller operation over the entire angle-of-attack range in the case of the pusher models.

8. The slipstreams at the tail locations were well defined, especially with the pusher models, and had approximately the same diameters as the propellers. In the case of the four-engine pusher, there appeared to be a definite shearing of the slipstream due to the trailing vortex sheet.

9. The largest observed variation in downwash angle across the elevator hinge line was 15° for the case of the two-engine pusher model, T_c' having a value of 0.435. The values of q/q_0 across the elevator hinge line for the same case varied between 1.0 and 3.2.

LANGLEY MEMORIAL AERONAUTICAL LABORATORY,
NATIONAL ADVISORY COMMITTEE FOR AERONAUTICS,
LANGLEY FIELD, VA., *August 24, 1939.*

REFERENCES

1. DeFrance, Smith J.: The N. A. C. A. Full-Scale Wind Tunnel. T. R. No. 459, N. A. C. A., 1933.
2. Theodorsen, Theodore, and Silverstein, Abe: Experimental Verification of the Theory of Wind-Tunnel Boundary Interference. T. R. No. 478, N. A. C. A., 1934.
3. Silverstein, Abe, and Katzoff, S.: Experimental Investigation of Wind-Tunnel Interference on the Downwash behind an Airfoil. T. R. No. 609, N. A. C. A., 1937.
4. Lesley, E. P., Worley, George F., and Moy, Stanley: Air Propellers in Yaw. T. R. No. 597, N. A. C. A., 1937.
5. Flachsbart, O., and Kröber, G.: Experimental Investigation of Aircraft Propellers Exposed to Oblique Air Currents. T. M. No. 562, N. A. C. A., 1930.
6. White, James A., and Hood, Manley J.: Wing-Fuselage Interference, Tail Buffeting, and Air Flow about the Tail of a Low-Wing Monoplane. T. R. No. 482, N. A. C. A., 1934.
7. Silverstein, Abe, and Katzoff, S.: Aerodynamic Characteristics of Horizontal Tail Surfaces. T. R. No. 688, N. A. C. A., 1940.
8. Goett, Harry J., and Reeder, J. P.: Effects of Elevator Nose Shape, Gap, Balance, and Tabs on the Aerodynamic Characteristics of a Horizontal Tail Surface. T. R. No. 675, N. A. C. A., 1939.
9. Silverstein, Abe, and Katzoff, S.: Design Charts for Predicting Downwash Angles and Wake Characteristics behind Plain and Flapped Wings. T. R. No. 648, N. A. C. A., 1939.